Potential energy surface, kinetics, and dynamics study of the $Cl+CH_4 \rightarrow HCl+CH_3$ reaction

Cipriano Rangel, Marta Navarrete, Jose C. Corchado, and Joaquín Espinosa-García[a)]
Departamento de Química Física, Universidad de Extremadura, 06071 Badajoz, Spain

(Received 4 November 2005; accepted 30 January 2006; published online 24 March 2006)

A modified and recalibrated potential energy surface for the gas-phase $Cl+CH_4 \rightarrow HCl+CH_3$ reaction is reported and tested. It is completely symmetric with respect to the permutation of the four methane hydrogen atoms and is calibrated with respect to updated experimental and theoretical stationary point properties and experimental forward thermal rate constants. From the kinetics point of view, the forward and reverse thermal rate constants and the activation energies were calculated using the variational transition-state theory with semiclassical transmission coefficients over a wide temperature range of 150–2500 K. The theoretical results reproduce the available experimental data, with a small curvature of the Arrhenius plot which indicates the role of tunneling in this hydrogen abstraction reaction. A dynamics study was also performed on this PES using quasiclassical trajectory (QCT) calculations, including corrections to avoid zero-point energy leakage along the trajectories. First, we found a noticeable internal energy in the coproduct methyl radical, both in the ground-state $[CH_4\ (v=0)]$ and vibrationally excited $[CH_4\ (v=1)]$ reactions. This CH_3 internal energy was directly precluded in some experiments or oversimplified in previous theoretical studies using pseudotriatomic models. Second, our QCT calculations give HCl rotational distributions slightly hotter than those in experiment, but correctly describing the experimental trend of decreasing the HCl product rotation excitation in going from HCl $(v'=0)$ to HCl $(v'=1)$ for the CH_4 $(v=1)$ reaction. Third, the state specific scattering distributions present a reasonable agreement with experiment, although they tend to make the reaction more forward and backward scattered than found experimentally probably because of the hotter rotational distribution and the deficiencies of the QCT methods. © *2006 American Institute of Physics*. [DOI: 10.1063/1.2179067]

I. INTRODUCTION

Potential energy surfaces (PESs) play a central role in the analysis of the kinetics and dynamics of reactive systems, and their construction is a process in continuous evolution, closely related to the development of high-level theoretical methods, functional forms more adequate to represent the nuclear motion, and the appearance of new experimental data.

In 1996 our group[1] reported for the first time an analytical PES for the title reaction, which was modified and updated in 2000 (Ref. 2) to correct the deficiencies of the earlier PES-1996. PES-2000 was symmetric with respect to any permutation of the four methane hydrogens, yielded rate constants in good agreement with the experimental data, and remarkably improved the CH_4/CD_4 kinetic isotope effects (KIEs) compared to the experimental values. From a dynamics point of view, it was found that excitation by one quantum of the C–H stretching and the umbrella bend modes of methane accelerate the forward reaction rates, whereas for thermal reactions in the products the Cl–H stretch mode will appear vibrationally unexcited, while the CH_3 umbrella mode will appear vibrationally excited. These conclusions about the population of the vibrational states agreed with the experimental data of Zare and co-workers.[3–6]

However, since we constructed this surface, we have observed three major drawbacks in this symmetric PES-2000. First, it has been experimentally observed that this reaction yields a rotationally cold Cl–H product,[4,5,7,8] while it gives a rotationally hotter HCl product. Second, in the calibration process we used the LCT3 method[9] to describe the tunneling effect of a large curvature, but one year later, Fernandez-Ramos and Truhlar[10] found that this method overestimates this effect, proposing a new method, LCT4, to correct this deficiency. Third, although the rate constants were in good agreement with the experimental data, the $^{12}CH_4/^{13}CH_4$ KIEs were too high compared to those of the experiment,[11–13] 1.141 against 1.066 at 300 K As is well known, this KIE is thought to have a great influence on the isotopic fractionation of tropospheric and stratospheric CH_4. In addition, the presence of very stable complexes in the entrance and exit channels caused some problems in conventional quasiclassical trajectory (QCT) methods.[14,15]

In the present work, to correct the deficiencies of PES-2000, we report the construction of a new analytical surface for the title reaction, denominated PES-2005. The article is structured as follows: in Sec. II, high-level electronic structure calculations are performed to study possible complexes in the entry and exit channels, which are sensitive parameters in the calibration process. In Sec. III, first, the development and calibration of the new PES-2005 is described and, second, the PES-2005 is tested against experimental and theo-

[a)]Electronic mail: joaquin@unex.es

retical values. The kinetics results using the variational transition-state theory (VTST) are presented in Sec. IV, while Sec. V presents a dynamical study using the QCT method. Section VI presents a comparison between both surfaces, PES-2000 and PES-2005, emphasizing the differences between them, and finally Sec. VII presents the conclusions.

For the sake of clarity it is necessary to distinguish between building and testing along the text. In fact, in the first step we build the PES for this reaction as an analytical potential energy surface describing the complete reactive system, from reactants to products, as a whole. This PES is calibrated by a combination of high-quality electronic structure calculations and the VTST. In the second step, we test this PES. We attempt to compare its predictions to experiment via the VTST for kinetic magnitudes (such as kinetic isotope effects) and via QCT calculations for dynamic magnitudes (such as reactive cross sections, product rotovibrational distributions, or scattering angular distributions), dealing with both the ground-state and the vibrationally excited methane.

II. ELECTRONIC STRUCTURE CALCULATIONS: INTERMEDIATE COMPLEXES

The title reaction is a prototype of a hydrogen abstraction reaction from alkanes by halides.

$$X + RH \rightarrow HX + R \quad (X = F, Cl, Br, I).$$

While the reactants, products, and saddle point for the $Cl+CH_4 \rightarrow HCl+CH_3$ reaction are well characterized, there is some controversy about the existence of stable intermediate complexes in the entry and exit channels.[8,16–23] Therefore, our goal in this section is to study these intermediate complexes using the Gaussian 3 (G3) theory[24] as implemented in GAUSSIAN 98.[25] In the entry channel we located a van der Waals complex close to the reactants, with a C···Cl bond distance of 3.588 Å at the MP2(full)/6-31G(d) level and where the Cl atom points toward the face of the CH_4 tetrahedron. The methane bond lengths and bond angles are close to those of the isolated CH_4. This complex presents a stabilization enthalpy at 0 K of -1.4 kcal mol^{-1} with respect to reactants. To assess the error limit of the G3 theory for this reaction, we have also calculated the heat of reaction (0 K) because a comparison with experiment is available. From the corresponding enthalpies of formation (at 0 K) an experimental value of ΔH_r (0 K) $= +1.0$ kcal mol^{-1} is obtained. With the G3 theory we obtain a value of $+0.4$ kcal mol^{-1}. Therefore, within this error limit, the van der Waals complex in the entry channel seems to have a real existence. This result agrees with a recent theoretical study[27] using a very high *ab initio* level, CCSD(T)/aug-cc-pVTZ, which found a C···Cl bond distance of 3.3 Å and a stabilization energy of -1.0 kcal mol^{-1}, taking into account the basis set superposition error.

There is some more theoretical information about the possible complex in the exit channel. In this channel we located a hydrogen bond complex with a productlike structure, $H_3C\cdots H-Cl$, with a C···H bond distance of 2.336 Å at the MP2(full)/6-31G(d) level and a stabilization enthalpy at 0 K of -0.7 kcal mol^{-1} with respect to the products. Therefore, taking into account the error limit of the G3 theory for this reaction, this low stability calls into question the existence of this complex. Chen *et al.*[21] found a similar complex (in geometry and stabilization) using the G1 theory, but the larger error limit of the G1 theory, namely, 1.5 kcal mol^{-1} for this reaction, makes the stability of the product complex questionable. Later, Duncan and Truong[28] located a similar complex using a density functional theory (DFT) method, BH&HLYP/6-311G(d,p), with a stabilization enthalpy at 0 K of -3.6 kcal mol^{-1}, which is of the order of the error limit of this DFT method for this reaction. In summary, we conclude that the existence of this product complex is questionable, and if it does exist it must have such a low stabilization energy that it has a negligible influence on the kinetics and dynamics of this reaction.

Finally, also in the exit channel, Gutman and co-workers[16–20] proposed a complex reaction mechanism in which the alkyl radical forms a complex with the halogen of XH, followed by a rotation of the hydrogen, giving a $H_3C\cdots X-H$ complex, named the X complex. Chen *et al.*[21–23] carried out a theoretical study of these reactions with different halogens using a variety of *ab initio* calculations, concluding that the X complex postulated by Gutman and coworkers could not be found. In this present work we located the X complex at the MP2(full)/6-31G(d) level, with a C···Cl bond length of 3.638 Å and a very small stabilization enthalpy of ΔH (0 K) $= -0.2$ kcal mol^{-1} at the G3 theory. Given the abovementioned error limit, we conclude that either the existence of the X complex is questionable or it does not exist.

In brief, based on our G3 calculations and taking into account the chemical accuracy (± 1 kcal mol^{-1}), we conclude that the existence of these complexes in the entry and exit channels is an open scientific question even today.

III. POTENTIAL ENERGY SURFACE

The $Cl+CH_4 \rightarrow HCl+CH_3$ polyatomic reaction consists of a hydrogen abstraction reaction from methane to yield the CH_3 radical, with a slow change in the geometry of the CH_3 group from pyramidal to planar along the reaction path. The functional form is the same as those of the PES-2000, and therefore will not be repeated here. Basically, it consists of four LEP (London-Eyring-Polanyi) stretching terms (str) augmented by out-of-plane (op) bending and valence (val) bending terms, with the form[29]

$$V = V_{str} + V_{op} + V_{val}. \quad (1)$$

It is important to note that this PES, as in the case of the PES-2000, is symmetric with respect to the permutation of the methane hydrogen atoms, a feature that is especially interesting for dynamics calculations.

Once the functional form is selected, the calibration process used in this work had several iterative steps, each one with a different objective. In the first step, we changed the parameters of the PES related to the geometric, energetic, and vibrational properties of the reactants and products, so that the geometries, endothermicity, and vibrational frequen-

TABLE I. Reactant and product properties (distances in angstrom, frequencies in cm^{-1}) calculated using the PES-2005 analytical surface.

System	R(C–H)	R(Cl–H)	Frequencies
CH_4[a]	1.094		3050 (t), 2884 1534 (e), 1369 (t)
CH_3[b]	1.094		3178 (e), 3005 1241 (e), 589
ClH[c]		1.275	3014

[a]Experimental values from Ref. 26: $CH_4(T_d)$=1.091 Å, 3019 (t), 2917, 1534 (e), 1306 (t).
[b]Experimental values from Ref. 26: $CH_3(D_{3h})$: 1.079 Å, 3184 (e), 3002, 1383 (e), 580.
[c]Experimental values from Ref. 30: ClH($C_{\infty v}$): 1.275 Å, 2991 cm^{-1}.

cies agree reasonably well with the available experimental data. Especial caution was taken to reproduce the slightly stable intermediate complexes in the entry and exit channels according to the previous *ab initio* calculations. Note that these complexes were not considered in our previous PES-2000 surface, with consequences for the HCl rotational distribution that will be analyzed below (Sec. VI). In the second step, since experimental information is not available for the saddle point, we refitted some parameters of the PES in order to reproduce the characteristics of the *ab initio* calculated saddle point, in particular, the geometry, barrier height, and the vibrational frequencies, with especial care for the imaginary frequency. Finally, since a main objective in this work was to analyze dynamical details of the reaction (importance of tunneling, rate temperature dependence, KIEs, reactant and/or product vibrorotational excitations, scattering angles, etc.), as the third step of our calibration, we refitted some of the parameters of the analytical PES in order to reproduce the whole set of experimental thermal forward rate constants. Obviously, this process represented considerable computational and personal efforts because 33 adjustable parameters were considered.

A. Test of consistency of the calibration

The results of the final fit are listed in Table I for the reactants and products, and in Table II for the saddle point. In general, the reactant and product properties agree very well with the experimental data,[26,30] with the most significant difference being 0.02 Å for the C–H bond length in the methyl radical. With respect to the vibrational frequencies, the small differences found balance out between reactants and products, yielding an enthalpy of reaction at 0 K of 0.9 kcal mol^{-1}, in close agreement with the experimental value[26] of 1.0 kcal mol^{-1}.

In the entry channel we found a van der Waals complex stabilized by 0.1 kcal mol^{-1} with respect to the reactants and with the chlorine atom pointed towards the face of the CH_4

TABLE II. Saddle point properties.

			Electronic structure calculations			
Parameter[a]	PES-2005[b]	PES-2000[c]	TTBGS[d]	DD[e]	DT[f]	Best[g]
$R^{\neq}$ (CH)	1.095	1.098	1.086	1.078	1.077	1.080
$R^{\neq}$ (CH′)	1.348	1.389	1.388	1.375	1.443	1.359
$R^{\neq}$ (ClH′)	1.394	1.356	1.431	1.452	1.431	1.451
ΔE	6.3	6.1	7.5[h]	7.6[h,i]	9.7[h]	6.8[h]
ΔH_0	0.9	0.9	2.2[h]	2.7[h]	4.4[h]	2.2[h]
$\Delta E^{\neq}$	7.6	7.7	8.8[h]	9.7[h]	10.7[h]	8.4[h]
$\Delta H^{\neq}$ (0 K)	2.4	3.1	4.4[h]	5.7[h]	6.3[h]	4.5[h]
Frequencies						
1,2	3093 (e)	3039 (e)	3295 (e)	3305 (e)	3328 (e)	3303 (e)
3	2961	2910	3118	3132	3162	3131
4,5	1333 (e)	1372 (e)	1449 (e)	1448 (e)	1468 (e)	1457 (e)
6	1022	1126	1227	1213	1211	1223
7,8	764 (e)	782 (e)	874 (e)	958 (e)	920 (e)	923 (e)
9	552	732	572	511	541	519
10,11	330 (e)	312 (e)	324 (e)	378 (e)	385 (e)	337 (e)
F	782i	760i	949i	1262i	996i	1136i

[a]Distances in angstrom, frequencies in cm^{-1}, energies in kcal/mol. H′ is the abstracted hydrogen. Symmetry C_{3v}.
[b]This work.
[c]Reference 2.
[d]Reference 31. MP2-SAC//MC-311G(2d,d,p) energies and geometries with MP2/MC-311G(2d,d,p) frequencies.
[e]Reference 32. MP2/TZ+2P level.
[f]Reference 28. DFT/6-311G(d,p) level.
[g]Reference 2. CCSD(T)/IB//MP2/pTZ level with scaled MP2/MC-311G(2d,d,p) frequencies for the saddle point (scale factor 0.96) and experimental frequencies for the reactants and products.
[h]We added the +0.8 kcal/mol contribution from the spin-orbit interaction to all energies in this table to provide a consistent comparison.
[i]Single-point CCSD(T)/cc-pVQZ energy calculations from Ref. 32.

TABLE III. Thermal forward rate coefficients for the $Cl+CH_4 \rightarrow HCl+CH_3$ reaction.

	Theory			Experiment					
T (K)	CUS/μOMT	CUS/μOMT3[a]	PES-2000[b]	Ref. 42	Ref. 43	Ref. 44	Ref. 45	Ref. 46	Refs. 3, 6, and 47
150	1.7(−15)[c]	3.0(−15)	3.0(−15)						
180	6.4(−15)	1.0(−14)	8.6(−15)					6.3(−15)	
200	1.2(−14)	1.8(−14)	1.4(−14)	1.1(−14)		1.1(−14)		1.2(−14)	
250	4.1(−14)	5.4(−14)	4.3(−14)	4.1(−14)		4.3(−14)		4.4(−14)	
300	9.9(−14)	1.2(−14)	9.9(−14)	1.0(−13)		1.0(−13)	9.4(−14)		9.3(−14)
400	3.4(−13)	3.9(−13)	3.4(−13)	3.5(−13)		3.1(−13)	3.4(−13)		3.0(−13)
500	8.2(−13)	8.8(−13)	8.1(−13)	8.8(−13)		8.2(−13)	7.5(−13)		6.5(−13)
600	1.6(−12)	1.7(−12)	1.6(−12)						1.3(−12)
800	4.1(−12)	4.3(−12)	4.3(−12)						3.0(−12)
1000	8.3(−12)	8.5(−12)	4.9(−12)						
1100	1.1(−11)	1.1(−11)	6.9(−12)		1.1(−11)				
1500	2.7(−11)	2.7(−11)	1.9(−11)		3.1(−11)				
2000	5.7(−11)	5.7(−11)	4.2(−11)						
2500	9.7(−11)	9.8(−11)	7.3(−11)						

[a]CUS/μOMT calculations on the PES-2005 surface based on LCT3 tunneling probabilities.
[b]Reference 2. CUS/μOMT calculations.
[c]1.7(−15) stands for 1.7×10^{-15} cm^3 molecule^{-1} s^{-1}.

tetrahedron, in agreement with previous *ab initio* calculations. Other less stable van der Waals complexes (less than 0.1 kcal mol^{-1} below the reactants) were also found with our PES, with the chlorine atom pointed toward the vertex or edge of the CH_4 tetrahedron. In the exit channel we found two van der Waals complexes, one with the reaction-path orientation, $H_3C\cdots H-Cl$ (stabilized by 0.3 kcal mol^{-1} with respect to the products and a C–Cl bond length of 3.575 Å), and another with the HCl rotated with respect to the previous complex, $H_3C\cdots Cl-H$ (stabilized by 0.4 kcal mol^{-1} with respect to the products and a C–Cl bond length of 4.419 Å). Undoubtedly, these very flat complexes obtained with our PES will have little or no influence on the kinetics and dynamics of the reaction, but they may affect the rotational excitation of the HCl product.

With respect to the saddle point geometry, in general the *ab initio* information[2,28,31,32] is well reproduced, with the most significant differences being the Cl–H′ bond (H′ being the abstracted hydrogen), which is shorter. In general, the *ab initio* data show that the Cl–H′ bond is longer than the C–H′ bond. This tendency is reproduced in this new PES-2005, which represents an improvement over our earlier PES-2000, which showed the inverse behavior. At the saddle point the length of the bond that is broken (C–H′) increases by 17%, and the length of the bond that is formed (Cl–H′) is only 9% larger than that at the products. This indicates that the reaction of the Cl atom with methane proceeds via a "late" transition state: i.e., it is a productlike transition state. This is the expected behavior that would follow from the endothermicity of the reaction. This saddle point is well characterized by one imaginary frequency. Its absolute value agrees with the value obtained with our earlier PES-2000, and is lower than the *ab initio* ones, but it is well known that the *ab initio* calculations overestimate the harmonic frequencies.

More interesting is the barrier height comparison (Table II). In our earlier work[2] different theoretical levels were analyzed, concluding that the classical barrier height is very sensitive to the extension of the one-electron basis set, a general problem in computational chemistry. Our best estimate was obtained by using Truhlar's "infinite basis" (IB) method,[33,34] which extrapolates CCSD(T) energies obtained by using correlation-consistent polarized double- and triple-zeta basis sets, cc-pVDZ and cc-pVTZ, and includes the increase in barrier height due to the spin-orbit effect of the Cl atom. With this method we obtained a classical barrier of 8.4 kcal mol^{-1} and an enthalpy of activation at 0 K (i.e., by including the zero-point energy) of 4.5 kcal mol^{-1}. However, given that our best estimate gives an enthalpy of reaction at 0 K of 2.2 kcal mol^{-1}, which overestimates the experimental value[26] by 1.2 kcal mol^{-1}, we can assume, *a priori*, a similar overestimation of the barrier height. Thus, we recommend a value of the enthalpy of activation at 0 K of 3.3 kcal mol^{-1}, in close agreement with the value obtained with our PES-2005 (2.4 kcal mol^{-1}).

At this point it is interesting to remember that the agreement in geometry, vibrational frequencies, and energy for the reactants, products, intermediate complexes, and saddle point is a consequence of the fitting procedure used, and it simply represents a check of the consistency of the parameterization.

The previous discussion about the barrier height, a single point on the whole surface, recalls the attention about the necessity of very high *ab initio* calculations to correctly describe a reactive system. Given that thousands of calculations are necessary to perform kinetics and dynamics calculations, this is even today a prohibitive task for polyatomic systems, increasing the problem with the molecular size. For instance, for comparison purposes exclusively, we have optimized the saddle point geometry at two modest levels, MP2/6-31G(d,p) and CCSD(T)/6-31G(d,p), obtaining classical barrier heights of 22.5 and 14.9 kcal mol^{-1}, respectively, very far from our recommended value of 8.4 kcal mol^{-1} (7.2 kcal mol^{-1} if the overestimation mentioned above is taken into account). Even a level as computationally de-

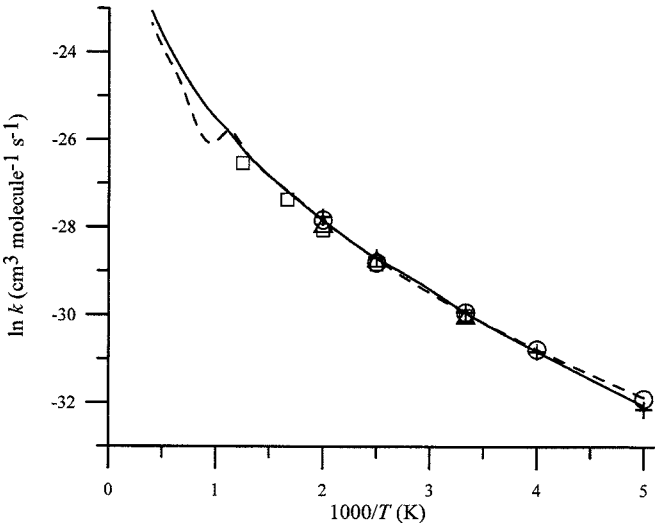

FIG. 1. Arrhenius plots of $\ln k$ (cm^3 $molecule^{-1}$ s^{-1}) for the forward thermal rate constants against the reciprocal of temperature (K) in the range 200–2500 K. Solid and dashed lines, our VTST values for the PES-2005 and PES-2000 surfaces, respectively. Experimental values as symbols: + (Ref. 42), △ (Ref. 43), ○ (Ref. 44), and □ (Refs. 3, 6, and 47).

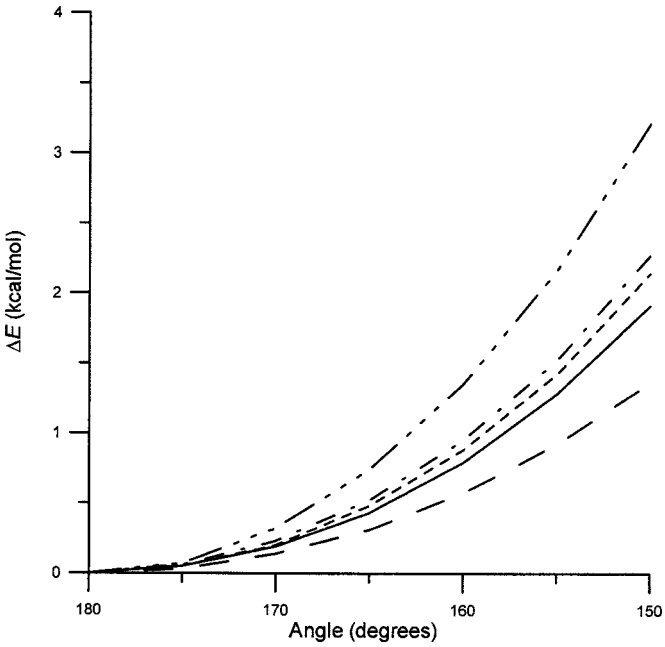

FIG. 2. Saddle point bending-energy curves (C–H–Cl) for the $Cl+CH_4$ reaction. The remaining internal coordinates have been kept fixed for the respective methods. Solid and dashed lines, our values for the PES-2005 and PES-2000 surfaces, respectively. Dotted line, CCSD(T)/cc-pVTZ *ab initio* calculations; dashed-dotted line, CCSD(T)/6-31G** *ab initio* calculations, and dashed-triple point line, MP2/6-31G** *ab initio* calculations. Note that the value of 180° corresponds to the saddle point.

manding as CCSD(T)/cc-pVTZ yields a barrier height of 9.6 kcal mol^{-1}, overestimating the recommended value by more than 2 kcal mol^{-1}. In view of this very demanding process, which usually requires a final *ad hoc* refit, an alternative for obtaining a global PES such as the one developed in the present work becomes essential for accurate kinetics and dynamics studies.

Another important test of consistency is the comparison with the experimental rate constants which were used in the calibration process. Starting from the saddle point geometry, we followed the reaction path towards both reactants and products, obtaining the minimum energy path[35] (MEP) in the range $s=\pm 3.0$ bohrs, s being the reaction coordinate. Along the MEP, we calculated vibrational frequencies after projecting out the motion along the reaction path using redundant internal coordinates.[36,37] With this information, we calculated the ground-state vibrationally adiabatic potential curve,

$$V_a^G(s) = V_{\mathrm{MEP}}(s) + \varepsilon_{\mathrm{int}}^G(s), \tag{2}$$

where $V_{\mathrm{MEP}}(s)$ is the classical energy along the MEP with its zero energy at reactants and $\varepsilon_{\mathrm{int}}^G(s)$ is the zero-point energy at s. Rate constants were estimated by using canonical variational transition-state theory (CVTST).[38,39] Quantum effects on motions transversal to the reaction path were included by using quantum-mechanical vibrational partition functions under the harmonic approach, while quantum effects in the motion along the reaction path were included by using the large curvature tunneling LCT4 method.[10] We used the microcanonical optimized multidimensional tunneling (μOMT) approach[40] in which, at each total energy, the larger of the small curvature tunneling (SCT) and large curvature tunneling (LCT) probabilities is taken as the best estimate. All kinetics calculations were performed using the general polyatomic rate constants code POLYRATE.[40] In the present work, we included the $^2P_{1/2}$ excited state of Cl (with an excitation energy[26] of 882 cm^{-1}) in the reactant electronic partition function, while the rotational partition functions were calculated classically. The analysis of the $V_a^G(s)$ curve showed the existence of two maxima and, therefore, the rate constants were finally calculated using the canonical unified statistical (CUS) model.[39,41]

Table III lists the variational CUS/μOMT thermal forward rate constants obtained with the PES-2005, together with the experimental and our previous PES-2000 rate constants for the temperature range 150–2500 K. Figure 1 shows the corresponding Arrhenius plot. As in the case of our PES-2000, the new parametrization of the surface, PES-2005, also reproduces the experimental data in the common temperature range, improving the agreement in the high-temperature range. Since the experimental thermal forward rate constants were used in the calibration process, again this represents simply another check on the consistency of the parametrization. Note that both the PES-2000 and PES-2005 rate constants were obtained using the μOMT methods for tunneling, but in the PES-2000 case the μOMT method employed was based on the LCT3 method for large-curvature tunneling. The μOMT tunneling coefficients of the PES-2005 calculations are based on the more recent LCT4 tunneling probabilities. For comparison, Table III also shows the PES-2005 rate constants computed using LCT3 tunneling probabilities in the μOMT calculations. The largest difference is seen, as expected, at 150 K, where tunneling is more important, but the two rates differ by less than 75%, while the same calculations with the PES-2000 give a factor of 6.5 of the difference between LCT3- and LCT4-based μOMT

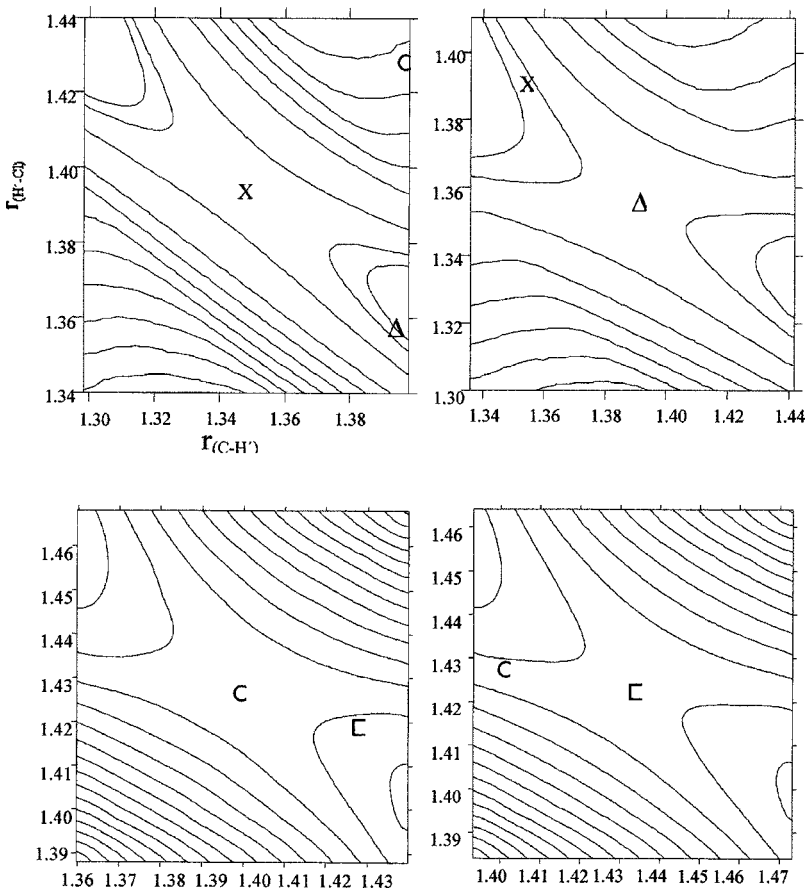

FIG. 3. Contour plots of the saddle point zone for the PES-2005 surface (first panel), PES-2000 surface (second panel), MP2/6-31G** *ab initio* level (third panel), and CCSD(T)/6-31G** *ab initio* level (fourth panel). The symbols ×, △, ○, and □ mean the respective saddle point at each level. The contours are shown at 0.1 kcal mol^{-1} increments, with the maximum value at the saddle point. When in a panel a symbol does not appear, this means that it is outside the represented range of distances. The axis labels are the same for the four plots.

tunneling factors. The relatively small difference in the PES-2005 surface between both methods is an advantage of the new surface, since it is well known that both the LCT3 method may overestimate tunneling,[10] especially at high energies, and the LCT4 may underestimate it,[48] especially at low energies. Therefore, the fact that our surface gives similar results using LCT3 and LCT4 suggests that this overestimation or underestimation of tunneling has little effect when using this surface and that the calibration process would have given a similar surface if we had used the LCT3 method. In any case, in the rest of the paper we will use the LCT4 tunneling probabilities for the μOMT calculations, although it is necessary to note that the kinetic isotope effects show little dependence on the large-curvature tunneling method used (see Sec. IV C).

B. Test of consistency of the new PES: Comparison with *ab initio* calculations

In order to confirm the accuracy and behavior of our analytical PES, we calculated a grid of configurations using *ab initio* calculations in sensitive zones of the reaction, such as the bending of the linear approach, and the saddle point zone. It is well known that there is a correlation between the bending frequency of the collinear saddle point (C–H′–Cl) and the product Cl–H′ rovibrational distribution.[49–51] Schatz and co-workers[50,51] found that surfaces having the same saddle point but different dependences of the energy on the bending angle showed very different rotational excitations in the products, concluding that looser saddle points imply hotter rotations. To test this energy dependence of the C–H′–Cl bending angle we carried out *ab initio* calculations at three levels, MP2/6-31G(d,p), CCSD(T)/6-31G(d,p), and CCSD(T)/cc-pVTZ, comparing them with the values from our analytical PES and our previous PES-2000 (Fig. 2). The new PES-2005 is more repulsive than the previous PES-2000, and *a priori*, a rotationally colder product is expected. This is one of the goals of this work. With respect to the *ab initio* calculations, the MP2 curve shows the most repulsive behavior. When the level of calculation increases, MP2/6-31G$(d,p)\rightarrow$CCSD(T)/6-31G$(d,p)\rightarrow$CCSD(T)/cc-pVTZ, the bending curve approaches our newest results.

With respect to the saddle point, Fig. 3 shows contour plots in the neighborhood of the saddle point using the new PES-2005 and, for comparison, the previous PES-2000 and two *ab initio* methods, MP2/6-31G(d,p) and CCSD(T)/6-31G(d,p). First, the four contour plots show a qualitative agreement, describing the reaction valley in a similar way, although the PES-2000 surface looks flatter than the *ab initio* and PES-2005 surfaces. Second, we observe that the location of the saddle point is strongly dependent on the level used. Note that these modest *ab initio* levels were used only for comparison purposes and, therefore, a direct comparison of the geometric results from these levels and the surface is irrelevant. Finally, taking as reference the new PES-2005, we observe that the PES-2000 saddle point is close, while the *ab initio* calculations give a looser saddle point.

TABLE IV. Reverse rate coefficients for the $Cl+CH_4 \rightarrow HCl+CH_3$ reaction.

	Theory		Experiment		
T (K)	CUS/μOMT	PES-2000[a]	Ref. 45	Ref. 51	Ref. 52
150	7.0(−15)[b]	10.6(−15)			
180	1.2(−14)	1.5(−14)			
200	1.6(−14)	1.8(−14)			
250	2.8(−14)	2.7(−14)			
300	4.0(−14)	3.7(−14)	4.8(−14)	2.0(−14)	
400	6.7(−14)	6.3(−14)	8.6(−14)	4.9(−14)	1.9(−14)
500	9.8(−14)	9.4(−14)	1.2(−13)		4.0(−14)
600	1.3(−13)	1.3(−13)			6.7(−14)
800	2.1(−13)	2.2(−13)			
1000	3.2(−13)	1.9(−13)			
1500	7.3(−13)	5.3(−13)			
2000	1.4(−12)	1.1(−12)			
2500	2.3(−12)	1.8(−12)			

[a]Reference 2. CUS/μOMT calculations. Note that the values in the original paper were incorrectly multiplied by 2.
[b]7.0(−15) stands for 7.0×10^{-15} cm^3 molecule^{-1} s^{-1}.

IV. KINETICS RESULTS AND DISCUSSION

We begin by testing the PES-2005 surface analyzing kinetic magnitudes, namely, the reverse rate constants (which have not been used in the calibration process) and the kinetic isotope effects.

A. Reverse rate constants

Table IV lists the CUS/μOMT thermal reverse rate constants, the scarce experimental data, and our PES-2000 results for the temperature range 150–2500 K. Our results agree well with the latest experimental values by Russell *et al.*[45] both in the values and in their temperature dependence. Note that the rate constants and their temperature dependence are significantly different in older experimental measurements,[52,53] which can be taken as a confirmation of the values of Russel *et al.* At this point it is useful to recall that only the forward rate constants were used in the calibration process.

The activation energies at 298 K (from slopes of the Arrhenius plots from 293 and 303 K) are 2.7 and 1.1 kcal mol^{-1} for the forward and reverse reactions, respectively. Using these theoretical activation energies, a value of 1.6 kcal mol^{-1} is obtained for the enthalpy of reaction at 298 K, in agreement with the experimental value from enthalpies of formation,[26] $\Delta H_r^{298\ \mathrm{K}}=1.6$ kcal mol^{-1}. This result is encouraging, although it was to be expected since all transition-state properties cancel out, as does the barrier shape.

B. Curvature terms, $B_{k,F}(s)$

Along the MEP the coupling terms $B_{k,F}(s)$ measure the coupling between the reaction coordinate (F) and the orthogonal bound modes (k). These coupling terms are the components of the reaction-path curvature $\kappa(s)$ defined as

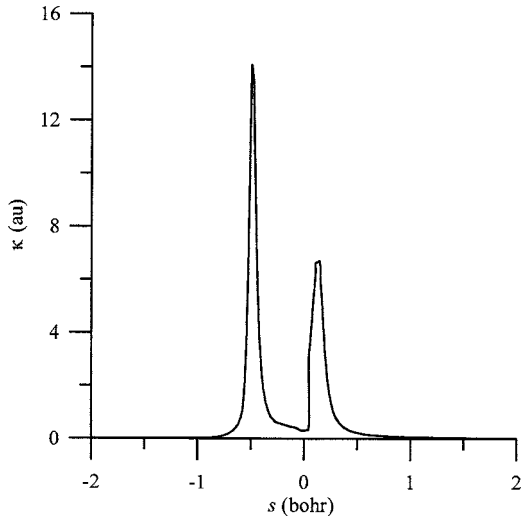

FIG. 4. Reaction-path curvature κ as a function of reaction coordinate s.

$$\kappa(s)=\left\{\sum [B_{k,F}(s)]^2\right\}^{1/2}, \tag{3}$$

and they control the nonadiabatic flow of energy between these modes and the reaction coordinate.[54–56] They will allow us to calculate accurate semiclassical tunneling factors and to give a qualitative explanation of the possible excitation of reactants and/or products, i.e., dynamical features, which are another sensitive test of the new surface. Figure 4 shows the curvature of the reaction path as a function of s. This figure shows the same behavior as reported with our previous PES-2000,[2] and it will not be repeated here. In brief, we shall note that the first peak in the entrance channel ($s=-0.405$ bohr) is due to the strong coupling of the reaction path to the CH_4 reactive stretch and the umbrella bend modes, while the second peak in the exit channel ($s=+0.070$ bohr) is due to the coupling of the reaction path to the Cl–H stretch and the CH_3 bend modes. However, as in the case of the PES-2000, there is not enough energy available to excite by one quantum the Cl–H stretch mode, al-

TABLE V. $^{12}C/^{13}C$ kinetic isotope effects for the forward reaction.

	KIE		
T (K)	PES-2005[a]	PES-2000[b]	Expt.
200	1.100	1.216	
250	1.078	1.173	1.069[c]
300	1.067	1.141	1.066[c,d],1.062[e],1.058[f]
400	1.055	1.099	
500	1.047	1.074	
600	1.040	1.060	
800	1.035	1.043	
1000	1.032	1.051	
1500	1.027	1.038	
2000	1.026	1.034	
2500	1.021	1.031	

[a]This work, CUS/μOMT calculations.
[b]Reference 2.
[c]Reference 11.
[d]Reference 12.
[e]Reference 57.
[f]Reference 13.

TABLE VI. $^{12}C/^{14}C$ kinetic isotope effects for the forward reaction.

	KIE	
T (K)	PES-2005[a]	Expt.[b]
200	1.22	1.16
250	1.19	1.14
300	1.17	1.13
400	1.14	1.11
500	1.11	1.09
600	1.10	1.08
800	1.08	1.06
1000	1.07	1.05
1500	1.06	1.05
2000	1.05	1.05
2500	1.04	1.05

[a]This work, CUS/μOMT calculations.
[b]Estimated value, Ref. 59.

though there is enough energy to excite by one quantum the CH_3 umbrella mode. Therefore, for thermal reactions the Cl–H stretch mode will appear vibrationally unexcited, while the CH_3 umbrella mode will appear vibrationally excited. These qualitative results agree with those of our previous PES-2000 and of experiments,[3–6] and they will be analyzed in more detail in the next dynamic study.

C. Kinetic isotope effects

In order to complete the test of the new surface we shall calculate the KIEs, which provide a sensitive test of several features of the shape of the surface (barrier height and width, and zero-point energy near the dynamics bottleneck). Six sets of KIEs (two more than those in the previous PES-2000 study) were calculated on this surface (Tables V–X)—

TABLE VII. CH_4/CD_4 kinetic isotope effects for the forward reaction.

	KIE		
T (K)	PES-2005[a]	PES-2000[b]	Expt.
200	49.6	87.7	
250	20.7	29.3	
295	11.8	14.9	16.4[c]
298	11.5	14.3	18.5,[d]12.2,[e]14.7[f]
300	11.2	14.0	
304	10.8	13.3	10.9[g]
400	5.1	5.6	5.2[g]
500	3.2	3.3	
600	2.4	2.4	
800	1.7	1.6	
1000	1.5	0.8	
1500	1.3	1.4	
2000	1.2	1.3	
2500	1.1	1.2	

[a]This work, CUS/μOMT calculations.
[b]Reference 2.
[c]Reference 60.
[d]Reference 61.
[e]Reference 62.
[f]Reference 13.
[g]Reference 63.

TABLE VIII. CH_4/CH_3D kinetic isotope effects for the forward reaction.

	KIE		
T (K)	PES-2005[a]	PES-2000[b]	Expt.
200	2.12	2.63	
250	1.87	2.22	1.58[c]
295	1.71	1.97	1.36[d]
298	1.70	1.96	1.51,[c]1.47,[e]1.54[f]
300	1.69	1.95	
304	1.66	1.94	
400	1.47	1.61	
500	1.34	1.43	
600	1.26	1.32	
800	1.15	1.20	
1000	1.09	0.99	
1500	1.08	1.12	
2000	1.05	1.09	
2500	1.03	1.07	

[a]This work, CUS/μOMT calculations.
[b]Reference 2, CUS/μOMT.
[c]Reference 64.
[d]Reference 60.
[e]Reference 13.
[f]Reference 61.

$^{12}CH_4/^{13}CH_4$, $^{12}CH_4/^{14}CH_4$, CH_4/CD_4, CH_4/CH_3D, CH_4/CH_2D_2, and CH_4/CHD_3—for the temperature range 200–2500 K.

With the new parametrization of the surface, the calculated $^{12}CH_4/^{13}CH_4$ KIEs are in much better agreement with the experimental data in the temperature range that has been studied experimentally, and with previous theoretical values.[58] Note that this was another of the aims of the present work. The $^{12}CH_4/^{14}CH_4$ KIEs (Table VI) were not studied with our previous PES-2000, and experimental data are not available. The only information is an estimate by Michelsen.[59] With the present PES-2005 we obtain an excellent agreement with Michelsen's estimate. The agreement be-

TABLE IX. CH_4/CH_2D_2 kinetic isotope effects for the forward reaction.

	KIE		
T (K)	PES-2005[a]	PES-2000[b]	Expt.
200	5.00	4.56	
250	3.77	3.56	
298	3.07	2.93	1.43,[c] 2.45,[d] 2.38[e]
300	3.04	2.91	
400	2.21	2.16	
500	1.80	1.76	
600	1.57	1.53	
800	1.34	1.29	
1000	1.22	0.87	
1500	1.10	1.19	
2000	1.07	1.12	
2500	1.03	1.10	

[a]This work, CUS/μOMT calculations.
[b]Reference 2, CUS/μOMT.
[c]Reference 62.
[d]Reference 13.
[e]Reference 61.

TABLE X. CH_4/CHD_3 kinetic isotope effects for the forward reaction.

	KIE	
T (K)	PES-2005[a]	Expt.
200	13.02	
250	8.08	
298	5.66	4.73,[b] 5.26[c]
300	5.59	
400	3.33	
500	2.41	
600	1.96	
800	1.53	
1000	1.34	
1500	1.15	
2000	1.09	
2500	1.06	

[a]This work, CUS/μOMT calculations.
[b]Reference 13.
[c]Reference 61.

tween these two sets of values can be taken as an indication of the accuracy of the values reported for this KIE.

The calculated CH_4/CD_4 KIEs (Table VII) agree with some of the experimental values (304 and 400 K), but they are lower than the more recent experimental value at 298 K. This underestimation of the KIE may be due to the use of the harmonic approximation to calculate the vibrational partition functions in both isomers, since the lowest vibrational frequencies of the CD_4 isomer make the CD_4+Cl reaction more likely to be affected by anharmonicity, and it is known that anharmonicity usually decreases the rate constants. Thus, including anharmonicity effects is expected to lower the CD_4+Cl rate constant, but to increase the values of the CH_4/CD_4 KIEs.

We have also calculated the CH_4/CH_3D KIEs (Table VIII). For the $Cl+CH_3D$ case, two reactions must be considered

$$Cl + CH_3D \rightarrow DCl + CH_3$$

$$\rightarrow HCl + CH_2D,$$

with symmetry factors of 1 and 3, respectively. The total rate constant corresponds to the sum of these two partial reactions. Our results improve considerably the previous PES-2000 and are closer to the experimental data, although the KIEs are still slightly overestimated.

Table IX lists the values of the CH_4/CH_2D_2 KIEs, which consist of two reactions

$$Cl + CH_2D_2 \rightarrow DCl + CH_2D$$

$$\rightarrow HCl + CD_2H,$$

both with a symmetry factor of 2. The present results are similar to those obtained with our PES-2000 and are reasonably close to the most recent experimental data,[13,61] which correct noticeably the only previous value.[62]

Finally, we calculated the CH_4/CHD_3 KIEs (Table X), which consist of the reactions

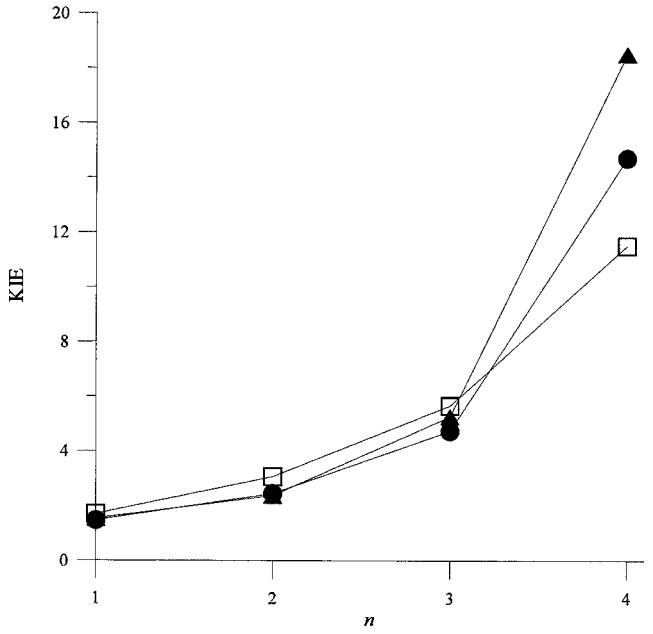

FIG. 5. Theoretical (□, this work) and experimental (●, Ref. 13; ▲, Ref. 61) CH_4/CD_nH_{4-n} KIEs at 298 K as a function of the number of substituted hydrogens, n.

$$Cl + CHD_3 \rightarrow DCl + CHD_2$$

$$\rightarrow HCl + CD_3,$$

with symmetry factors 3 and 1, respectively. The present results agree quite well with the experimental values,[13,61] although they also are slightly overestimated.

In brief, carbon KIEs are in very good agreement with experimental values, while deuterium KIEs seem to be slightly overestimated except in the CH_4/CD_4 case, where the theoretical values are lower than the experimental measurements. This is shown graphically in Fig. 5, where the theoretical and experimental[13,61] KIEs at 298 K are plotted against the number of hydrogen atoms substituted by deuterium. The theoretical values agree reasonably well with the experimental measurements except in the CD_4 case, where the calculations cannot reproduce the sudden increase in the KIE with the substitution of the only hydrogen atom in CD_3H. As mentioned above, the greater anharmonicity of the deuterium reactions may be responsible for this behavior. In the other three KIEs (CH_3D, CH_2D_2, and CHD_3) the larger weight of the H channel compared to that of the D channel compensates for the anharmonic effect.

V. DYNAMICS RESULTS AND DISCUSSION

After testing kinetic magnitudes in the previous section, in this section we attempt to compare the dynamics predictions from the PES-2005 surface to experiment via QCT calculations, dealing with both the ground-state and the vibrationally excited methane.

QCT calculations[65–67] were carried out using the VENUS 96 code,[68] which was customized to incorporate our analytical PESs. The accuracy of the trajectory was checked by the conservation of total energy and total angular momentum. The integration step was 0.1 fs, with an initial separation

between the Cl atom and the methane center of mass of 8.5 Å. For the reactions with methane and perdeuteromethane in their ground states, the vibrational and rotational energies were obtained as a thermal sampling at 300 K, while for the methane vibrationally excited only the rotational energy was thermally sampled also at 300 K. To simulate the experimental conditions,[4,5] we considered a relative translational energy of 0.159 eV for methane and 0.179 eV for CD_4.

First, the maximum value of the impact parameter b_{max} was computed for each of three analyzed reactions of chlorine with $CH_4(v=0)$, $CD_4(v=0)$, and $CH_4(v=1)$ by calculating batches of 10 000 trajectories at fixed values of the impact parameter b, systematically increasing the value of b until no reactive trajectories were obtained. The b_{max} values for the $CH_4(v=0)$, $CD_4(v=0)$, and $CH_4(v=1)$ reactions are, respectively, 3.0, 2.5, and 3.5 Å. The reaction probability N_r/N is the ratio of the number of reactive trajectories and the total number of trajectories, while the reactive cross section is defined as

$$\sigma_r = \pi b_{max}^2 (N_r/N). \quad (4)$$

Second, in order to compare experimental and theoretical QCT results for each reaction considered in this work, namely, ground-state CH_4, ground-state CD_4, and vibrationally excited CH_4, batches of 100 000 trajectories were calculated, where the impact parameter b was sampled by

$$b = b_{max} R^{1/2}, \quad (5)$$

with R being a random number in the interval [0, 1].

A serious drawback of the QCT calculations is related with the question of how to handle the quantum-mechanical zero-point energy (ZPE) problem in the classical mechanics simulation.[69–85] Many strategies have been proposed to correct this quantum-dynamics effect (see, for instance, Refs. 69–76, 81, and 82, and references therein), but no completely satisfactory alternatives have emerged. Here, we employed a pragmatic solution, the so-called passive method,[76] and discarded all the trajectories that fulfill at least one of the following conditions.

(i) The initial total energy is lower than the classical energy of the saddle point of the reaction plus its harmonic ZPE, since in the quantum-mechanical world it would never overcome the barrier to reaction.
(ii) The vibrational energy of the products is lower than their ZPE, since in the quantum-mechanical world this is the lowest limit.

After having discarded these trajectories, we perform a simple histogram binning of the resulting trajectories. Since we are removing all the trajectories with energies below the ZPE of the products, we consider the system to be in the vibrational ground state whenever the vibrational energy is lower than the energy of the first excited vibrational state, while it is in the first excited state whenever the vibrational energy lies above the energy of the first excited state and below the energy of the second excited state. In other words, we take as a vibrational quantum number the truncated integer of the real vibrational actions. However, the rotational number is taken, as usual, as the integer nearest to the computed rotational action. This is what we call histogram binning with simple ZPE correction (HB-ZPE), and is the method that we will use in our calculations unless otherwise noted.

Before beginning the analysis of the results obtained in this dynamics study, there are two relevant issues concerning the comparison of theoretical and experimental values (i) the role of the impact parameter and (ii) the available energy channeled into the internal excitation (rotation plus vibration) of the products HCl and CH_3.

With respect to the first point, it is well known[86] that, in general, the impact parameter controls the rotational excitation and the scattering distributions of the products. Thus, low impact parameters lead to predominantly backward scattered products, usually accompanied by cold rotational distributions and collinear transition-state structures. This corresponds to the typical rebound mechanism. However, high impact parameters lead to predominantly forwarded products, corresponding to the stripping mechanism also called peripheral collisions.[87] For the title reaction, Simpson *et al.*[5] found that when the CH_4 (CD_4) is in its vibrational ground state the product HCl ($v'=0$) is formed with a cold rotational distribution and is strongly backscattered. These experimental data, in conjunction with the collinear Cl–H–C transition-state structures from theoretical studies, indicate a direct, rebound mechanism, with low impact parameters. However, for the CH_4 vibrationally excited, Simpson *et al.*[4] found that the HCl product shifts to more sideways [HCl ($v'=0$)] and more forward [HCl ($v'=1$)] regions, and these data were interpreted in terms of a stripping mechanism, where the larger available energy opens the "cone of acceptance" and leads to larger impact parameters.

The second relevant issue is the available energy channeled into the internal excitation of the products.[88] Thus, the experimental observations by Simpson *et al.*[4,5] were based on the photoloc technique, in which the experimental speeds were inverted to obtain the scattering distribution assuming no methyl excitation. However, recently, Bass *et al.*[89] found that there are inherent problems with this inversion method, and although the inversion analysis provides an exact fit to the data, the results are inappropriate. They concluded that the radical product internal excitation must be taken into account, and this modifies the scattering distribution. With respect to previous theoretical dynamics results, except for the study of Wang *et al.*,[78] two very recent QCT studies[14,15] using the previous PES-2000 and the study of Rudic *et al.*,[90] all other studies[91–96] used pseudotriatomic or pseudotetratomic models, which, as was previously analyzed, give an oversimplified view of polyatomic reaction dynamics.

A. Cl+CH_4 (v=0) and Cl+CD_4 (v=0) reactions

The QCT reactive cross section σ_r for the Cl+CH_4 ($v=0$) and Cl+CD_4 ($v=0$) reactions are, respectively, 0.28 ± 0.02 Å^2 and 0.05 ± 0.01 Å^2, with reaction probabilities of 0.96% and 0.25%. This low reactivity of perdeuter-

omethane with respect to methane agrees with the KIEs analyzed in Sec. IV of this paper and represents an additional test of consistency of the new PES.

In both reactions the population of the vibrationally excited HCl (DCl) product, $v'=1$, was negligible, in agreement with experimental results,[5] while the umbrella mode of the methyl radical (589 cm^{-1}) was found to be vibrationally excited in some reactive trajectories. Note that this vibrational excitation of the CH_3 radical was already predicted in our kinetic coupling term analysis (Sec. IV B). This indicates that the internal excitation of the radical product, CH_3 in this case, plays an important role in the dynamics of the reaction. In fact, the available energy is partitioned into the relative transnational (f'_T), vibrational (f'_v) and rotational (f'_R) internal energies of the products HCl and CH_3, with the following average fractions: $\langle f'_T\rangle=0.31\pm0.01$, $\langle f'_V\rangle_{HCl}=0.32\pm0.02$, $\langle f'_R\rangle_{HCl}=0.09\pm0.01$, $\langle f'_V\rangle_{CH_3}=0.17\pm0.02$, and $\langle f'_R\rangle_{CH_3}=0.11\pm0.01$. These are similar to the results for the CD_4 reaction: $\langle f'_T\rangle=0.31\pm0.02$, $\langle f'_V\rangle_{DCl}=0.28\pm0.03$, $\langle f'_R\rangle_{DCl}=0.08\pm0.01$, $\langle f'_V\rangle_{CD_3}=0.20\pm0.03$, and $\langle f'_R\rangle_{CD_3}=0.13\pm0.01$. First, recently, Murray *et al.*[8] experimentally measured the fraction of the total available energy partitioned into the HCl rotation, with a value $\langle f'_R\rangle_{HCl}=0.09\pm0.01$, in excellent agreement with our results. Zhou *et al.*[97] noted an important kinetic isotope effect on the transnational energy of the products, which is not observed in the present work. Thus, they obtained $\langle f'_T\rangle=0.60$ and 0.31 for the CH_4 and CD_4 reactions, respectively. Only the latter experimental value agrees with our results. Second, these results strongly contrast with the experimental observations, which found a negligible CH_3 vibrational excitation, although they agree with the recent observations for the "cousin" $Cl+C_2H_6$ reaction by Bass *et al.*[89] who found a noticeable internal excitation (22% on the average of the available energy) of the ethyl radical. These results indicate that the methyl radical is not a simple spectator in this reaction, and therefore the triatomic or tetratomic models used theoretically or experimentally are unreliable, oversimplifying the complex dynamics of this polyatomic reaction.

As we mentioned above, we analyze our results by applying a simple passive ZPE correction to a simple histogram binning (HB-ZPE). However, it has been pointed out that the binning procedure can affect significantly the conclusions of QCT calculations.[98] Therefore, we also tested the widely used Gaussian-weighted binning procedure.[98,99] In addition, we checked the influence of the way that reactive trajectories with vibrational energies below the ZPE of products are eliminated. Thus, since in the HB-ZPE procedure we only discard the trajectories with a final value of the vibrational energy below the total ZPE of the products (i.e., the sum of the ZPEs of HCl and CH_3), we tried a more stringent criterion discarding all the trajectories that lead either to a HCl with a vibrational energy below its ZPE or to a CH_3 with a vibrational energy below its ZPE. This way we only count the reactive trajectories for which the nascent CH_3 and HCl have vibrational energies above their respective ZPEs. This is what we call histogram binning with double ZPE correction (HB-DZPE). Finally, we checked the influence of treating the rotational levels in the same way as the vibrational levels, i.e., once we have obtained rotational numbers, they are not rounded to the nearest integer, but are truncated to their integer part (rounded to the lower integer value). This option was checked because systems with a rotational fractional number between 0.5 and 1.0 have a rotational energy below the energy of the first excited state, and in the quantum-mechanical world they can only be in the ground state, while the usual histogram binning puts them in the first excited state. Given the different binning methods used to calculate the j' rotational number, which convert the continuum of the classical world to the discrete information of the quantum world, we estimate an error limit of ±1. Finally, we compare these binning procedures with the simplest method, the widely used histogram binning with no ZPE correction whatsoever. The results of applying these binning procedures to the analysis of the nascent HCl $(v'=0,j')$ rotational population distribution are shown in Fig. 6.

From Fig. 6(a) we can see that the histogram binning with no ZPE correction gives rise to a wide distribution of j', while including the simple ZPE correction leads to a distribution that peaks at $j'=1$, with the $j'=2$ and $j'=3$ levels being almost equally populated. Using the Gaussian weighting instead of the HB-ZPE has a relatively small effect: although the $j'=3$ level is the most populated, the $j'=1$ and $j'=2$ levels are also almost equally populated. It has to be noted, though, that the Gaussian binning has the disadvantage that it effectively reduces the number of reactive trajectories (since some trajectories have an almost zero weight), and more trajectories are required to give the same statistical accuracy as the HB-ZPE method.[100] This is why the HB-ZPE method is our chosen method.

From Fig. 6(b) one can see that applying a double ZPE correction (once for the HCl product and once for the CH_3 product) also has a minor effect, slightly raising the population of the $j'=2$ level and slightly decreasing the population of the $j'=3$ level (compared to the HB-ZPE results). The truncation of the value of j to the nearest lower integer decreases the population of the $j'=3$ level, leaving the $j'=1$ level clearly dominant. Note that the latter binning method is the only one that gives as many reactive trajectories as the HB-ZPE method, while not increasing the statistical uncertainties.

Therefore, since all the methods (except the histogram binning with no ZPE correction) give similar results, and ZPE-HB is the one that gives the smallest statistical error, in the remainder of the paper, except where noted, we will use it for our calculations. It has to be noted that, although we are only presenting the results for the rotational populations of the $Cl+CH_4$ $(v=0)$ reaction, we reached the same conclusion in all the cases, the differences being only significant in the rotational population of the CH_4 $(v=1)+Cl$ reaction, as will be discussed below.

The nascent HCl $(v'=0,j')$ rotational population distribution for the $Cl+CH_4$ $(v=0)\rightarrow HCl$ $(v'=0,j')+CH_3$ reaction is plotted in Fig. 7(a), together with theoretical and experimental results for comparison. The distribution was experimentally observed to be very cold, peaking at $j'=0$ (Ref. 5) or $j'=1$.[7,8] Previous reduced dimensionality QCT (Ref. 96) and quantum scattering[92,93] calculations confirmed

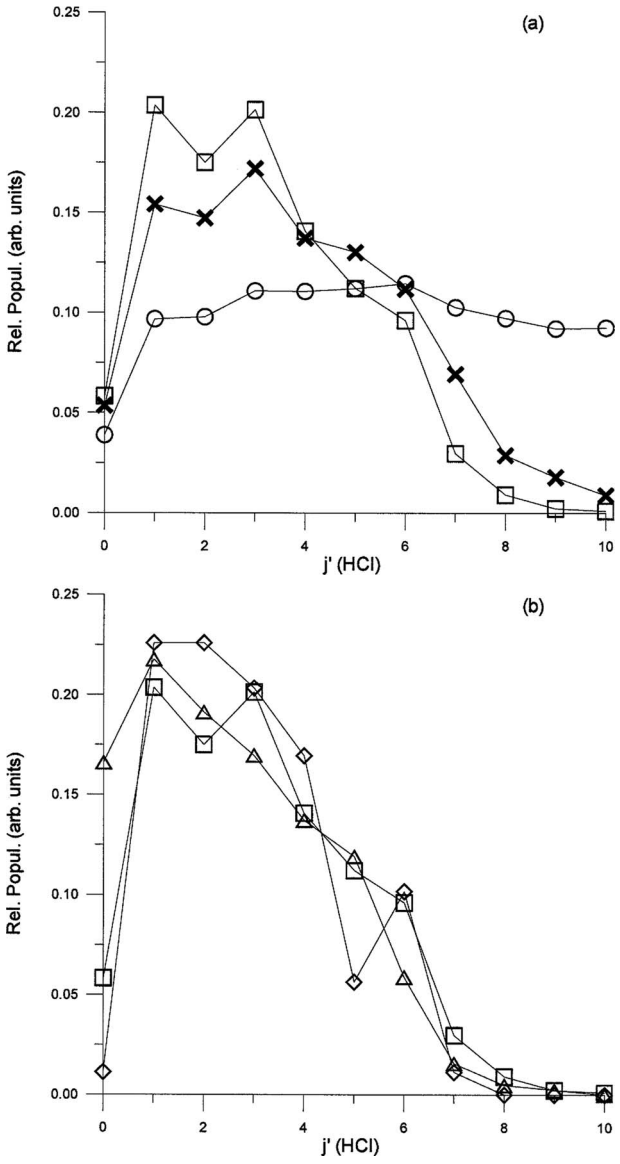

FIG. 6. Rotational populations for the $Cl+CH_4$ $(v=0)\rightarrow HCl$ $(v'=0,j')+CH_3$ reaction, which are computed using histogram binning taking into account all the reactive trajectories (○), histogram binning with simple ZPE correction (□), Gaussian binning (×), histogram binning with double ZPE correction (◇), and histogram binning with simple ZPE correction and truncated j values (△). The distributions are normalized so that the area under the common levels is the same. The figure has been divided into two panels for clarity.

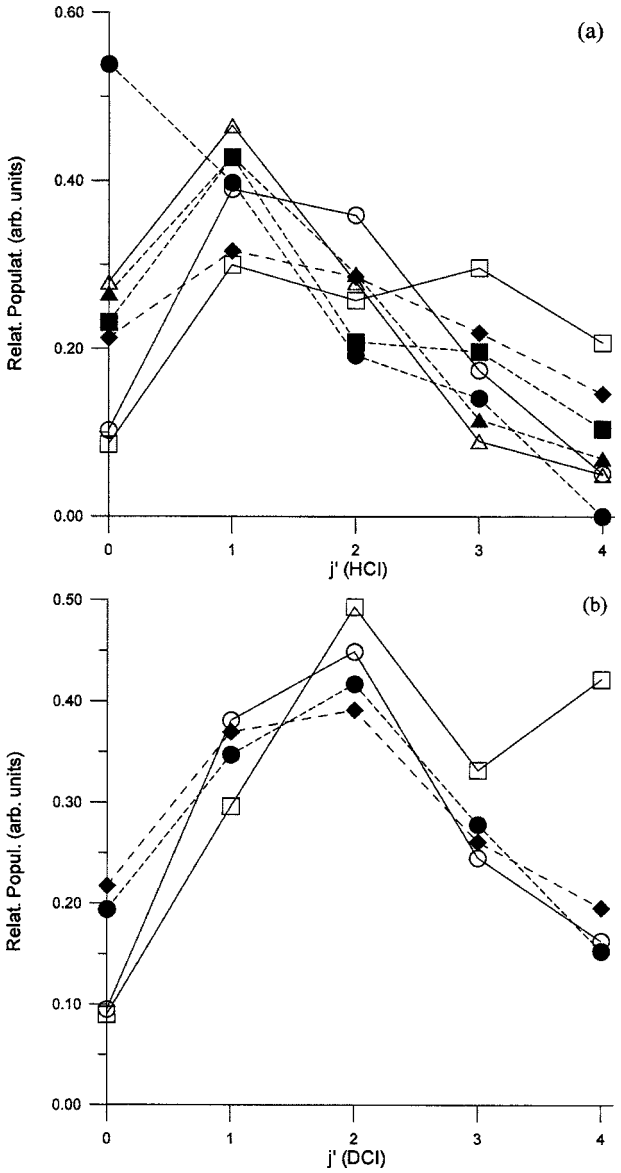

FIG. 7. Rotational populations for (a) CH_4 $(v=0)+Cl\rightarrow HCl$ $(v'=0,j')+CH_3$ and (b) CD_4 $(v=0)+Cl\rightarrow DCl$ $(v'=0,j')+CD_3$. Dashed lines are experimental values from Refs. 5 (●), 7 (■), 8 (▲), and 97 (♦), and solid lines are theoretical values from this work (□), Refs. 92 and 93 (△), and Ref. 96 (○). The distributions are normalized so that the area under the common levels is the same.

this finding, although these theoretical studies found a broader distribution. Our QCT calculations also give a broader distribution with similar populations of the levels with j' between 1 and 3. However, when the same rotational distribution is plotted for the perdeuteromethane reaction [Fig. 7(b)], the agreement between theory and experiment is better, both peaking at $j'=2$, although our distribution continues being broader. Given the collinear and tightly constrained transition-state structure obtained with our PES, the hotter rotational distribution of the HCl product may be due to the existence of the van der Waals complex in the exit channel, which as was analyzed previously, even being little stabilized, presents an incorrect C···Cl–H orientation. So, when the HCl product separates from the CH_3 coproduct the complex falls into this well, producing the rotation of the HCl product. Nevertheless, it is also possible that the hotter rotational distribution is an artifact of the QCT approach, since as noted elsewhere,[100–104] quantum-mechanical calculations tend to narrow and shift the rotational distributions. Moreover, an alternate binning method with j' being truncated to the lower integer, as discussed above, also gave a narrower distribution peaking at $j'=1$ (Fig. 6). Therefore, at this point we cannot say whether the hotter and wider rotational distributions are a drawback of the QCT method and binning procedures or of the surface.

Finally, we analyze the scattering angular distribution of the HCl $(v'=0,j')$ product (obtained as the differential cross sections computed by the Legendre moment method described in Ref. 105) as a function of j' (Fig. 8). It can be seen that for $j'=0$, the maximum of the differential cross section

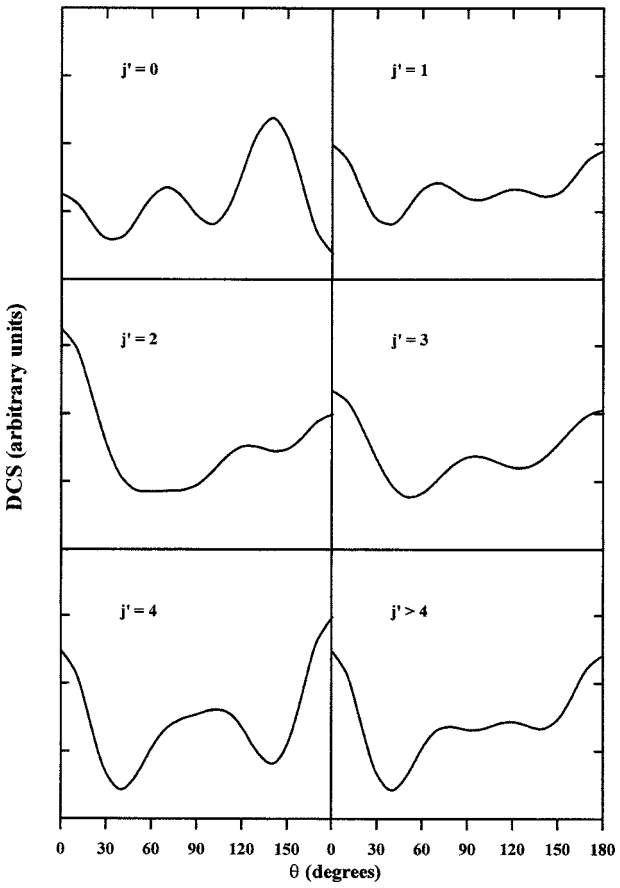

FIG. 8. Product angular distribution for the $Cl+CH_4$ $(v=0) \rightarrow HCl$ $(v'=0,j')+CH_3$ reaction, with $j'=0,1,2,3,4,\ldots$.

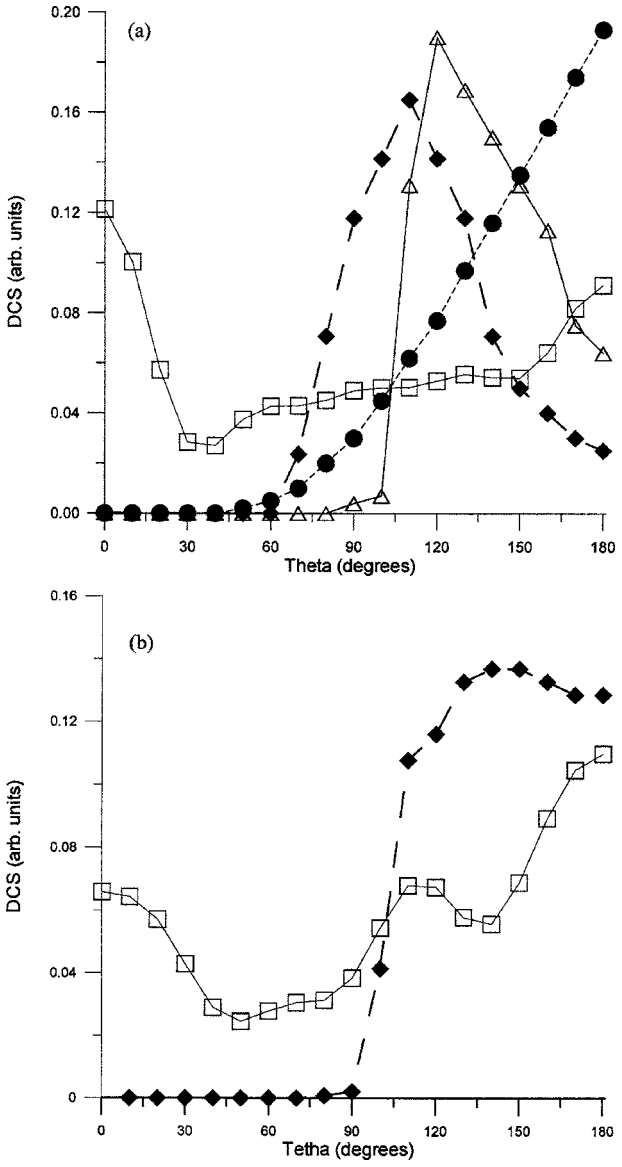

FIG. 9. Product angular distributions for (a) CH_4 $(v=0)+Cl \rightarrow HCl$ $(v'=0,j')+CH_3$ and (b) CD_4 $(v=0)+Cl \rightarrow DCl$ $(v'=0,j')+CD_3$. Dashed lines are experimental values from Refs. 5 (●) and 97 (◆), and solid lines are theoretical values from this work (□) and Refs. 92 and 93 (△). The scattering distributions are normalized so that the area under the common regions is the same.

(DCS) is located at 140°, with no backward scattering and little forward scattering. However, as we increase j', the forward and backward scattering increase, and the peak at 140° diminishes and shifts leading to a sideward scattering. However, the peaks at 0° and 180° are higher. As a result, when all the j' values are included [Fig. 9(a)], the scattering is predicted to be quite isotropic, although the forward scattering is dominant.

Experimentally, Simpson *et al.*[5] found for the perdeuterated reaction that the product DCl $(v'=0,j'=0)$ is strongly backscattered, with the differential cross section peaking at $\theta=180°$, and that the reaction with CH_4 presents a similar behavior. Those authors interpreted these observations in terms of a rebound mechanism dominated by small impact parameters. However, recently, Zhou *et al.*[97] revealed an interesting isotope effect in product angular distributions and a strong dependence on the energy of collision. At similar energies they found that for the $Cl+CD_4$ reaction the product angular distribution is backward, forming a swath in that hemisphere, while for the $Cl+CH_4$ reaction it is more sideways. Figure 9 compares the scattering distribution of the HCl $(v'=0,j')$ and DCl $(v'=0,j')$ with these experimental results and other previous theoretical studies.[92,93] Our QCT angular distributions for the unsubstituted reaction [Fig. 9(a)] are more isotropic and predict a forward scattering. However, as pointed out above, this is mainly due to the contribution of high values of j' that appear significantly populated in our calculations, while experimental results indicate a low population of these levels. Thus, if we compare our $j'=0$ DCS with the experimental values of Zhou *et al.*[97] we find a reasonable agreement. It can be expected that if the use of a quantum-mechanical method (instead of QCT) can predict a narrower rotational population peaking at $j'=0$ or $j'=1$, then the DCS will be more similar to the one we obtain for $j'=0$. Therefore, once again we cannot know for sure whether the discrepancy between the experimental results and our calculations is due to the PES-2005 surface or to the QCT and HB-ZPE binning methods.

This can be expected to hold for the $Cl+CD_4$ reaction. In this case, the agreement with the experiment is much better than in the previous case, but we now also find a significant forward scattering, contrary to experimental measurements [Fig. 9(b)]. Unfortunately, for this reaction the number of reactive trajectories is much smaller than for the Cl

$+CH_4$ reaction, and we cannot carry out the detailed study shown in Fig. 8. However, an analysis of the DCS for the $j'=2$ level (which is the most populated rotational level for this reaction) showed that, in agreement with the experiment, the predicted forward scattering is negligible, thus reinforcing the arguments of the previous paragraph: a method that can predict a narrower rotational distribution will probably give rise to better agreement in the DCS.

It is interesting to note that although we used the HB-ZPE procedure with a truncated j' value we were able to reproduce the experimental rotational populations much better [see Fig. 6 and 7(a)]; the truncation of j' has no effect at all on the calculation of the DCS for the HCl $(v'=0,j')$ product.

The difference between the older experimental results $(\theta=180°)$ (Ref. 5) and our QCT calculations $(\theta=140°)$ could be due to the way that the experimental data were inverted to obtain the scattering distribution (see Sec. VI). In the experimental process the CH_3 speed was excluded, and if this product would appear with internal excitation the differential cross section of the other product, HCl, would appear closer to the sideward region. In fact, we found this internal excitation with our PES, and so this shift from a pure backward region to a more sideways region is indeed observed with our PES.

B. Cl+CH_4 (v=1) reaction

For comparison with the experiment,[4] in our QCT calculations we have also excited the asymmetric stretching mode of methane of 3050 cm^{-1}, whose value agrees with the experimental one, 3019 cm^{-1}.

The reactive cross section obtained with our QCT calculations is 3.83 ± 0.02 $Å^2$, with a reaction probability of 9.95%. Therefore, the vibrational excitation of the stretching mode of methane increases the reactivity by a factor of 14, in good agreement with the experimental studies which estimate factors of 30 ± 15 (Ref. 4) or, more recently, 10 ± 5 (Ref. 106). This increase in the reactivity is the expected behavior for reactions with a late barrier,[107] such as that obtained with our PES, and it was already anticipated in our kinetic coupling term analysis (Sec. IV B). Note that the previous QCT calculations performed by Troya *et al.*[96] using a pseudotriatomic surface gave an increase in the reactivity by a factor of only 4.

In order to shed more light on this subject, we also calculated the coupling terms between vibrational modes, Bmm' (Corioli-type terms), which control the nonadiabatic flow of energy between vibrational modes. We found that although several modes seem to be coupled, one particular Bmm' term is especially large, the one that measures the coupling of the symmetric (ν_1) stretch and the umbrella (ν_4) modes, indicating that energy can flow between these modes in the entrance channel. Therefore the symmetric stretch and the umbrella bending modes do not preserve their adiabatic character along the reaction path, i.e., the reaction is not adiabatic. Note that although smaller, we also found a coupling between the ν_1 and ν_3 (asymmetric) stretch modes of methane in the entry valley, which questions the simple adiabatic picture of located and normal modes, i.e., the simple adiabatic picture. Therefore, one part of the energy originally deposited on the asymmetric mode flows to other modes. In the light of these observations, we can conclude that there is a noticeable intramolecular vibrational redistribution (IVR) and, therefore, both stretching states will be similarly populated in the entry channel. We have not attempted to improve upon this qualitative level of accuracy here, although this will be addressed in a future work.[108]

A second effect of the CH_4 vibrational excitation is on the energy partition in the products. As the energy available to the products is now greater, both the CH_3 and the HCl appear vibrationally excited. It was experimentally found[4,109] that approximately 30%–37% of the HCl product is formed in the first excited vibrational state $(v'=1)$ with a cold rotational distribution, while the remaining HCl is formed in the ground state $(v'=0)$ with a hotter rotational distribution. As has already been noted, in this experiment the internal excitation of the CH_3 coproduct is discarded, and therefore this radical is not considered. Previous QCT calculations[96] also discarded the methyl radical. Our QCT results indicate that, depending on the binning method, between 26% (histogram binning with no ZPE correction) and 11% (histogram binning with a double ZPE correction) of the HCl product is formed in the $v'=1$ state and that the CH_3 appears vibrationally excited. For the $Cl+CH_4\ (v=1)\rightarrow HCl\ (v'=0)+CH_3$ reaction the following average fractions of product energy are obtained: $\langle f'_T\rangle=0.30\pm0.01$, $\langle f'_V\rangle_{HCl}=0.21\pm0.01$, $\langle f'_R\rangle_{HCl}=0.17\pm0.03$, $\langle f'_V\rangle_{CH_3}=0.23\pm0.01$, and $\langle f'_R\rangle_{CH_3}=0.09\pm0.01$. For the $Cl+CH_4(v=1)\rightarrow HCl(v'=1)+CH_3$ reaction, the corresponding values are: $\langle f'_T\rangle=0.23\pm0.01$, $\langle f'_V\rangle_{HCl}=0.05\pm0.01$, $\langle f'_R\rangle_{HCl}=0.05\pm0.01$, $\langle f'_V\rangle_{CH_3}=0.58\pm0.02$, and $\langle f'_R\rangle_{CH_3}=0.09\pm0.01$. In the first case, we obtain a CH_3 umbrella mode vibrationally excited, mainly to $v'=2$. This result agrees with the quantum scattering study by Yu and Nyman,[92] but disagrees with the experimental one,[4] which indicates no vibrational excitation. In the second case, HCl $(v'=1)$, the available energy is enough to excite the CH_3 umbrella mode up to $v'=3$, the CH_3 bending mode $(1240\ cm^{-1})$ to $v'=1$ or the CH_3 umbrella and bending modes both to $v'=1$. As in the case of the CH_4 $(v=0)$ reaction, this result contrasts with both theoretical[96] and experimental[4] observations, which found that the vibrational excitation of the methyl radical is negligible. From the rotational average fractions of energy of the HCl product, 0.17 and 0.05 for HCl $(v'=0)$ and HCl $(v'=1)$, respectively, it is clear that the rotational distribution is hotter in the first case, in agreement with the experiment.[4,109] Next we analyze this rotational distribution population in more detail.

The QCT rotational population distributions for HCl $(v'=0,j')$ and HCl $(v'=1,j')$ are plotted in Figs. 10 and 11, respectively, along with experimental and other theoretical results for comparison. Both distributions were experimentally found[4] to be cold, peaking at $j'=1$ for the HCl $(v'=1)$ state, and somewhat hotter, $j'=3-4$, for HCl $(v'=0)$. For the HCl $(v'=0)$ state using the HB-ZPE binning we obtain a broad distribution peaking in region $j'=6-9$, while using the histogram binning with the double ZPE correction we obtained a narrower distribution peaking in region j'

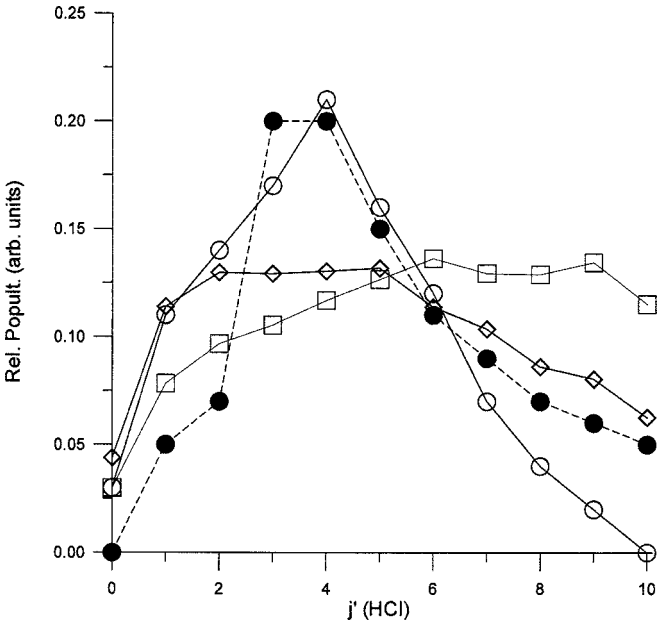

FIG. 10. Rotational populations for the Cl+CH$_4$ ($v=1$)→HCl ($v'=0,j'$)+CH$_3$. The dashed line represents experimental values from Ref. 4 (●), and solid lines are theoretical values from this work using the HB-ZPE binning procedure (□), the double ZPE binning procedure (◇), and Ref. 96 (○). The distributions are normalized so that the area under the common levels is the same.

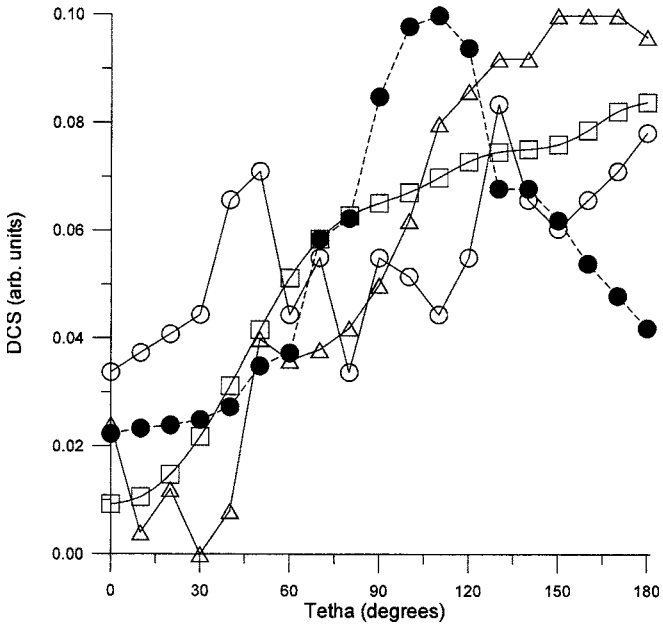

FIG. 12. Product angular distributions for Cl+CH$_4$ ($v=1$)→HCl ($v'=0,j'$)+CH$_3$. The dashed line represents experimental values from Ref. 4 (●), and solid lines are theoretical values from this work (□), Refs. 92 and 93 (△), and Ref. 96 (○). The scattering distributions are normalized so that the area under the common regions is the same.

=2–5, in good agreement with the experimental distribution which peaks at $j'=3$–4, although the latter is even narrower.

For the HCl ($v'=1$) state (Fig. 11), the distribution is narrower, peaking between $j'=2$–3 when the HB-ZPE binning is used, while the double ZPE correction once again narrows and shifts the distribution to colder rotational numbers, peaking at $j'=1$, in excellent agreement with experiment, although our QCT distributions are still broader. Our calculations, therefore, describe the experimental decrease in the HCl rotational excitation in going from HCl ($v'=0$) to HCl ($v'=1$). This result is coherent with the previously obtained rotational average fractions of energy, 0.17 and 0.05, indicating that the HCl is rotationally colder when the vibrational excitation increases.

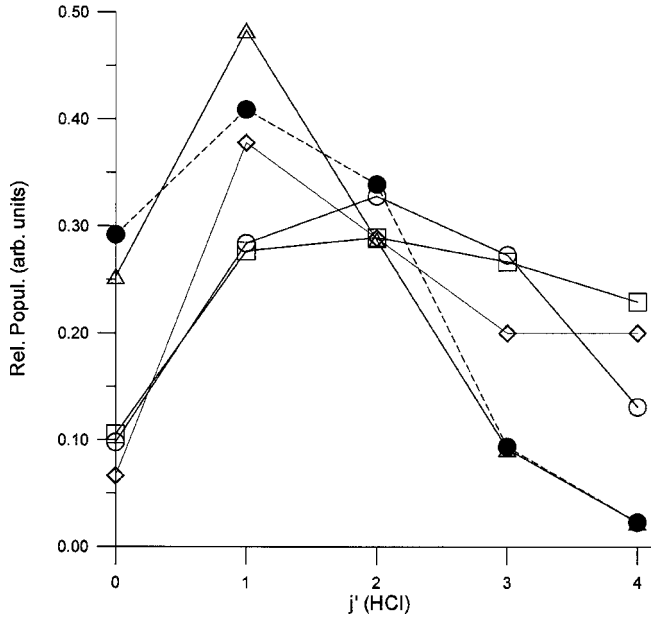

FIG. 11. Rotational populations for Cl+CH$_4$ ($v=1$)→HCl ($v'=1,j'$)+CH$_3$. The dashed line represents experimental values from Ref. 4 (●), and solid lines are theoretical values from this work using the HB-ZPE binning procedure (□), the double ZPE binning procedure (◇), Refs. 92 and 93 (△), and Ref. 96 (○). The distributions are normalized so that the area under the common levels is the same.

Finally, the angular distributions in terms of the DCS are plotted in Figs. 12–14 for the HCl ($v'=0,j'$) and HCl ($v'=1,j'$) reactions, computed using the HB-ZPE method. Note that the double ZPE correction significantly reduces the number of HCl ($v'=1,j'$) reactions, and our tests for the HCl ($v'=0,j'$) reaction show little effect of the double ZPE correction. For the first case, experimentally the HCl ($v'=0,j'$) product is back- and sidescattered, while previous QCT calculations[92] found a more isotropic distribution, and quantum scattering calculations[96] found that the products are mainly backward scattered. The present QCT calculations agree with the quantum results, although they have a more significant sidewards contribution. As was already analyzed, the differences between theory and experiment in our case could be due to the way the QCT state is analyzed (i.e., the binning procedure) or to the way the experimental data were inverted to obtain the angular distribution (see Sec. VI), where the methyl excitation is clearly precluded in the experiment.

For the Cl+CH$_4$ ($v=1$)→HCl ($v'=1,j'$)+CH$_3$ reaction, the measured[4] angular distribution depends on the HCl rotational excitation being sharply forward scattered for low j' (0–2) and becoming nearly equally forward-backward scattered for high j' (3 or higher). Previous theoretical studies, both QCT (Refs. 78 and 96) and quantum scattering[92] calculations, found only a qualitative agreement with the ex-

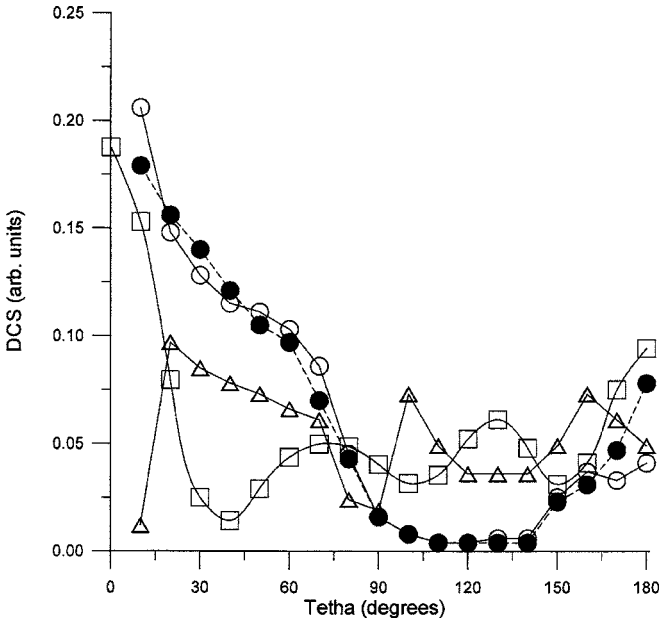

FIG. 13. Product angular distributions for $Cl+CH_4$ $(v=1)\rightarrow HCl$ $(v'=1,j'=1)+CH_3$. The dashed line represents experimental values from Ref. 4 (●), and solid lines are theoretical values from this work (□), Ref. 78 (△), and Ref. 96 (○). The scattering distributions are normalized so that the area under the common regions is the same.

periment, although in all cases they showed the evolution towards a more backward region with an increasing HCl rotational excitation. However, our QCT angular distributions are clearly forward and practically independent of the HCl rotational number, although the evolution towards a backward region is also observed, as can be seen from the average scattering angles in Table XI. Moreover, the tendency towards a forward distribution in the vibrationally excited methane is the expected behavior because the larger available energy opens the cone of acceptance, leading to larger impact parameters, i.e., a stripping mechanism.

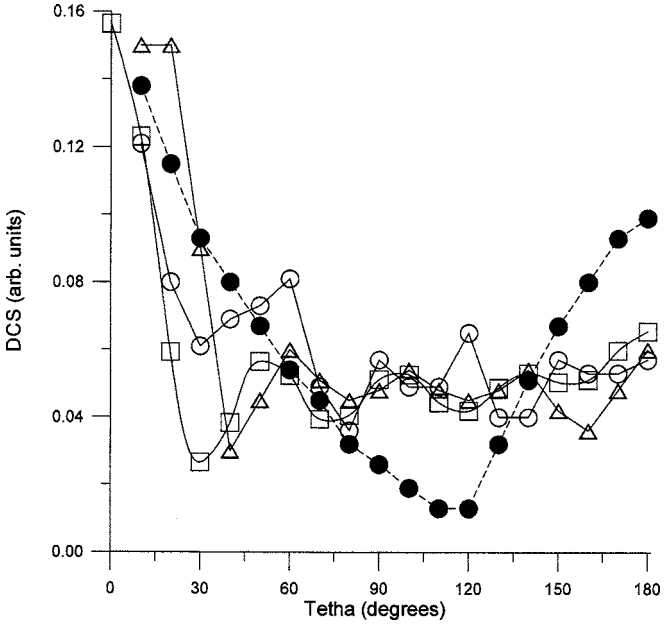

FIG. 14. The same as Fig. 13, but for the $Cl+CH_4$ $(v=1)\rightarrow HCl$ $(v'=1,j'=3)+CH_3$ reaction.

TABLE XI. Average scattering angle θ (in degrees) for the $Cl+CH_4$ $(v=1)\rightarrow HCl$ $(v'=1,j')+CH_3$ reaction.

Rotational number	θ	Method	Reference
$j'=1$	58.1	Expt.	3
$j'=3$	79.3		
$j'=1$	80.8	Theor. QCT	78
$j'=3$	83.1	(six-atom model)	
$j'=1$	60.2±2.0	Theor. QCT	96
$j'=3$	79.5±2.9		
$j'=1$	87.3±5.3	Theor. QCT	This work
$j'=3$	91.1±4.9		

VI. COMPARISON WITH THE EARLIER PES-2000

First, it is important to note that both surfaces, PES-2000 and PES-2005, are symmetric with respect to the permutation of the four hydrogens in methane, which is very important for dynamics calculations.

Second, the largest differences between the two surfaces are related to the answers that we are giving to the three issues posed in the Introduction, namely, HCl rotational excitation, better consideration of tunneling effect, and better description of the $^{12}C/^{13}C$ KIEs. The main results appear in Table XII. In the calibration process, we changed the old LCT3 method to estimate the tunneling effect by the newer LCT4 method. As the calibration criterion was to reproduce the experimental forward thermal rate constants in both sur-

TABLE XII. PES-2000 vs PES-2005. Kinetics and dynamics comparison.

	PES-200	PES-2005	Expt.
	Electronic structure[a]		
$\Delta E^{\neq}$	7.7	7.6	···
vi	760i	782i	···
ΔE (CR)	−3.1	−0.1	···
ΔE (CP)	−4.6	−0.3, −0.4	···
	Kinetics[b]		
k	9.9×10^{-14}	9.9×10^{-14}	1.0×10^{-13}
μOMT	3.33	3.64	···
KIE $^{12}C/^{13}C$	1.141	1.067	1.066
KIE CH_4/CD_4	14.0	11.2	12.2–18.5
	Dynamics[c]		
Reaction probability (%)	0.090	0.958	···
σ_r	0.025	0.281	···
Higher HCl j'	6	1–3	0–1
CH_4 $(v=1)/(v=0)$[d]	53	14	30±15, 10±5
HCl $(v'=1)/(v=0)$[e]	3	11–26	30–37

[a]$\Delta E^{\neq}$: classical barrier height (kcal/mol); vi: imaginary frequency (cm^{-1}); ΔE (CR): stabilization energy (kcal/mol) of the van der Waals complex in the entry channel, with respect to the reactants; ΔE (CP): stabilization energy (kcal/mol) of the van der Waals complex in the exit channel, with respect to the products.

[b]k; forward thermal rate constants at 300 K (cm^3 $molecule^{-1}$ s^{-1}); μOMT: tunneling factor, LCG3 method for the PES-2000, and LCG4 method for the PES-2005.

[c]Dynamics magnitudes for the $Cl+CH_4$ $(v=0)$ reaction, collision energy: 0.159 eV. σ_r: reactive cross section ($Å^2$); j': HCl rotational number; θ: scattering angle (degrees).

[d]Increase in reactivity upon excitation of the CH_4.

[e]Vibrational excitation in the HCl product for the $Cl+CH_4$ $(v=1)$ reaction.

faces, this change has no effect on the rate constants, but influences the $^{12}C/^{13}C$ KIEs, which agree much better with the experiment.

Third, undoubtedly the largest difference between the earlier PES-2000 and this new PES-2005 is related to the existence of very deep wells in the entry and exit channels for PES-2000, which noticeably modifies the QCT calculations. Our previous PES-2000 showed a deep van der Waals well in the entrance channel (3.1 kcal/mol stabilized with respect to the reactants). As a consequence, when in QCT calculations the Cl atom approaches the CH_4 molecule, the energy of the system lowers and the Cl atom orbits around the methane for a long time. During this time the chances are that a large amount of vibrational CH_4 energy is transferred to the Cl translational energy. Therefore, the reaction that takes place is the collision between a hot Cl and a methane molecule with a vibrational energy below its ZPE. These trajectories, however, are unacceptable, since they are artifacts of the QCT calculations and are not allowed in the quantized real world. In the exit channel, our PES-2000 also presented a van der Waals well which is deeper in this case (4.6 kcal/mol stabilized with respect to the products) and with an anomalous orientation, where the methyl radical bonds to the chlorine atom of HCl, $H_3C\cdots Cl-H$. Because of the depth of this well, when the trajectory leaves the transition-state zone the complex rapidly falls into the well with the incorrect orientation, producing a noticeable rotational excitation of the HCl product.

In this work we have analyzed the existence of these wells in the entry and exit channels by using high-level *ab initio* calculations (see Sec. II) and have concluded that they are very little stabilized with respect to the reactants or products, and consequently will have a little influence on the dynamics of this reaction. In our PES-2005 we found these complexes to be very flat (0.1 and 0.3–0.4 kcal mol^{-1}, respectively), reproducing the *ab initio* results, although the two complexes in the exit channel present opposite orientations. Consequently, a colder HCl rotational distribution is obtained with respect to our previous PES-2000, but it still slightly overestimates the experiment.

VII. CONCLUSIONS

In this work we have recalibrated our previous analytical potential energy surface (PES-2000) for the gas-phase $Cl+CH_4 \rightarrow HCl+CH_3$ reaction. The new surface, named PES-2005, is also semiempirical and, as calibration criteria, we use the theoretical and experimental stationary point properties (reactants, products, saddle point, and intermediate complexes) and the experimental thermal forward rate constants.

First, a kinetics study employing the variational transition-state theory (VTST) was performed. The forward and reverse thermal rate constants were calculated over the temperature range 150–2500 K. The agreement with experimental measurements is good over the whole temperature range, reproducing the curvature of the Arrhenius plot. This agreement between our VTST calculations and the experimental measurements encouraged us to perform an analysis of the kinetic isotope effects. These KIEs are a very sensitive test of features of the new surface, such as barrier height and width, zero-point energy, and tunneling effect. We found an excellent agreement for the very sensitive $^{12}CH_4/^{13}CH_4$ KIEs, a good agreement for the deuterium KIEs, and a moderate agreement for the perdeuteromethane reaction. The analysis of the reaction-path curvature (kappa factor) qualitatively shows that with CH_4 in its vibrational ground state only the CH_3 umbrella mode in the products could appear vibrationally excited, while the excitation of the C–H stretching mode in CH_4 accelerates the forward reaction rates. This qualitative prediction agrees with other theoretical and experimental results, and is quantitatively confirmed in our subsequent dynamics study. So the reaction-path curvature represents a point of connection between the kinetics and the dynamics.

Second, an extensive dynamics study employing quasiclassical trajectory (QCT) calculations was also performed on this surface, dealing with both the ground-state and vibrationally excited C–H stretching methane for the title reaction and its perdeuterated reactions. In this QCT study we explicitly considered the zero-point energy problem to avoid leakage along the trajectories. Confirming the qualitative conclusions of the reaction-path curvature analysis, it was found that the CH_3 product appears vibrationally excited, and that the excitation of the CH_4 stretching mode enhances the forward rate constants by a factor of 14, in agreement with experimental results which estimate factors of 30 ± 15 and, more recently, 10 ± 5.

For both the ground-state $[CH_4\ (v=0)]$ and the vibrationally excited state $[CH_4\ (v=1)]$ we find that the coproduct CH_3 radical presents a noticeable internal energy (rotation plus vibration): 23% for the $Cl+CH_4\ (v=0) \rightarrow HCl\ (v'=0,j')+CH_3$ reaction, 32% for the $Cl+CH_4\ (v=1) \rightarrow HCl\ (v'=0,j')+CH_3$ reaction, and 65% for the $Cl+CH_4\ (v=1) \rightarrow HCl\ (v'=1,j')+CH_3$ reaction. Therefore, the methyl radical does not behave as a simple spectator in the title reaction. For the subsequent comparison with the experiment or other theoretical works, it is important to note that this internal excitation of the methyl radical was not considered in the experiment and oversimplified in the previous theoretical studies, which used pseudotriatomic models. Bearing these considerations in mind, our QCT calculations give HCl rotational distributions slightly broader and hotter than those of the experiment by one or two units of j', although they correctly describe the experimental trend for the vibrationally excited methane $[CH_4(v=1)]$ reaction of decreasing the HCl rotation excitation in going from the HCl $(v'=0)$ to the HCl $(v'=1)$. With respect to the state specific scattering distributions, our QCT calculations agree only qualitatively with the experiment, our results peaking at more forward and backward regions.

In sum, our theoretical results show a good agreement with the experimental kinetics measurements (forward and reverse rate constants, activation energy, KIEs, and reaction-path curvature) and a moderate agreement with the wide spectrum of experimental dynamics measurements (vibrorotational excitation, available internal energy in products, and scattering distributions). This qualitative agreement lends support to the newly constructed polyatomic PES, although

there are some differences which may be due to the potential energy surface, of course, but also to the known limitations of the QCT method (especially the binning procedures) and/or problems with the way that the experimental data are inverted to obtain scattering angles assuming no methyl excitation.

VIII. SUPPLEMENTARY MATERIAL

As a supplementary material we report the optimized geometries and energies for all stationary points using the PES-2005 surface.[110]

ACKNOWLEDGMENTS

The authors would like to thank Diego Troya and Andy Ho for their helpful suggestions. This work was partially supported by the Junta de Extremadura, Spain (Project No. 2PR04A001.).

[1] J. Espinosa-García and J. C. Corchado, J. Chem. Phys. **105**, 3517 (1996).
[2] J. C. Corchado, D. G. Truhlar, and J. Espinosa-García, J. Chem. Phys. **112**, 9375 (2000).
[3] W. R. Simpson, A. J. Orr-Ewing, and R. N. Zare, Chem. Phys. Lett. **212**, 163 (1993).
[4] W. R. Simpson, T. P. Rakitzis, S. A. Kandel, A. J. Orr-Ewing, and R. N. Zare, J. Chem. Phys. **103**, 7313 (1995).
[5] W. R. Simpson, T. P. Rakitzis, S. A. Kandel, T. Lev-On, and R. N. Zare, J. Phys. Chem. **100**, 7938 (1996).
[6] A. J. Orr-Ewing, W. R. Simpson, T. P. Rakitzis, S. A. Kandel, and R. N. Zare, J. Chem. Phys. **106**, 5961 (1997).
[7] D. F. Varley and P. J. Dagdigian, J. Phys. Chem. **99**, 9843 (1995).
[8] C. Murray, B. Retail, and A. J. Orr-Ewing, Chem. Phys. **301**, 239 (2004).
[9] T. N. Truong, D.-H. Lu, G. C. Lynch *et al.*, Comput. Phys. Commun. **75**, 43 (1993).
[10] A. Fernandez-Ramos and D. G. Truhlar, J. Chem. Phys. **114**, 1491 (2001).
[11] G. Saueressig, P. Bergamaschi, J. N. Crowley, H. Fisher, and G. W. Harris, Geophys. Res. Lett. **22**, 1225 (1995).
[12] J. N. Crowley, G. Saueressig, P. Bergamaschi, H. Fisher, and G. W. Harris, Chem. Phys. Lett. **303**, 268 (1999).
[13] K. L. Feilberg, D. W. T. Griffith, M. S. Johnson, and C. J. Nielsen, Int. J. Chem. Kinet. **37**, 110 (2005).
[14] C. Rangel, J. C. Corchado, and J. Espinosa-García, J. Phys. Chem. A **109**, 8071 (2005).
[15] E. Garcia, C. Sanchez, A. Saracibar, and A. Lagana, J. Phys. Chem. A **108**, 8752 (2004).
[16] J. J. Russell, J. A. Seetula, R. S. Timonen, D. Gutman, and D. F. Nava, J. Am. Chem. Soc. **110**, 3084 (1988).
[17] J. J. Russell, J. A. Seetula, and D. Gutman, J. Am. Chem. Soc. **110**, 3092 (1988).
[18] D. Gutman, Acc. Chem. Res. **23**, 375 (1990).
[19] J. A. Seetula and D. Gutman, J. Phys. Chem. **94**, 7529 (1990).
[20] J. J. Russell and D. Gutman, J. Am. Chem. Soc. **112**, 1347 (1990).
[21] Y. Chen, E. Tschuikow-Roux, and A. Rauk, J. Phys. Chem. **95**, 9832 (1991).
[22] Y. Chen, A. Rauk, and E. Tschuikow-Roux, J. Phys. Chem. **95**, 9900 (1991).
[23] Y. Chen and E. Tschuikow-Roux, J. Phys. Chem. **97**, 3742 (1993).
[24] L. A. Curtiss, K. Raghavachari, P. C. Redfern, V. Rassolov, and J. A. Pople, J. Chem. Phys. **109**, 764 (1998).
[25] M. J. Frisch, G. W. Trucks, H. B. Schlegel *et al.*, GAUSSIAN 98 program, Revision A.7, Gaussian Inc., Pittsburg, PA, 1998.
[26] M. W. Chase, C. A. Davis, J. R. Downey, D. J. Frurip, R. A. McDonald, and A. N. Syverud, JANAF Thermochemical Tables, J. Phys. Chem. Reference Data Suppl. 1985 14.
[27] J. Klos, Chem. Phys. Lett. **359**, 309 (2002).
[28] W. T. Duncan and T. N. Truong, J. Chem. Phys. **103**, 9642 (1995); **109**, 3703(E) (1998).
[29] T. Joseph, R. Steckler, and D. G. Truhlar, J. Chem. Phys. **87**, 7036 (1987).
[30] G. Herzberg and K. B. Huber, *Constants of Diatomic Molecules*, Molecular Spectra and Molecular Structure Vol. 4 (Van Nostrand, Princeton, New Jersey, 1979).
[31] T. N. Truong, D. G. Truhlar, K. K. Baldridge, M. S. Gordon, and R. Steckler, J. Chem. Phys. **90**, 7137 (1989).
[32] K. D. Dobbs and D. A. Dixon, J. Phys. Chem. **98**, 12584 (1994).
[33] D. G. Truhlar, Chem. Phys. Lett. **294**, 45 (1998).
[34] P. L. Fast, M. L. Sánchez, and D. G. Truhlar, J. Chem. Phys. **111**, 2921 (1999).
[35] P. L. Fast and D. G. Truhlar, J. Chem. Phys. **109**, 3721 (1998).
[36] C. F. Jackels, Z. Gu, and D. G. Truhlar, J. Chem. Phys. **102**, 3188 (1995).
[37] Y.-Y. Chuang and D. G. Truhlar, J. Phys. Chem. A **102**, 242 (1998).
[38] B. C. Garrett and D. G. Truhlar, J. Am. Chem. Soc. **101**, 4534 (1979).
[39] D. G. Truhlar, A. D. Isaacson, and B. C. Garrett, in *Theory of Chemical Reaction Dynamics*, edited by M. Baer (CRC, Boca Raton, FL, 1985), Vol. 4, p. 65.
[40] Y.-Y. Chuang, J. C. Corchado, P. L. Fast, *et al.* POLYRATE, Version 8.0, University of Minnesota, Minneapolis, 1998.
[41] B. C. Garrett and D. G. Truhlar, J. Chem. Phys. **76**, 1853 (1982).
[42] M. S. Zahniser, B. M. Berquist, and F. Kaufman, Int. J. Chem. Kinet. **10**, 15 (1978).
[43] K. Takahashi, O. Yamamoto, and T. Inomata, Proc. Combust. Inst. **29**, 2447 (2002).
[44] W. B. DeMore, S. P. Sander, D. M. Golden, R. F. Hampson, M. J. Kurylo, C. J. Howard, A. R. Ravishankara, C. E. Kolb, and M. J. Molina, Jet Propulsion Laboratory Report No. 92-20, 1992 (unpublished).
[45] J. J. Russell, J. A. Setula, and D. Gutman, Int. J. Chem. Kinet. **20**, 759 (1988).
[46] J. V. Seeley, J. T. Jayne, and M. J. Molina, J. Phys. Chem. **100**, 4019 (1996).
[47] S. A. Kandel and R. N. Zare, J. Chem. Phys. **109**, 9719 (1998).
[48] J. A. Sansón, M. L. Sánchez, and J. C. Corchado, J. Phys. Chem. A **110**, 589 (2006).
[49] N. C. Blais and D. G. Truhlar, Chem. Phys. Lett. **118**, 379 (1985).
[50] G. C. Schatz, B. Amaee, and J. N. L. Connor, J. Chem. Phys. **92**, 4893 (1990).
[51] D. Troya, R. Z. Pascual, and G. C. Schatz, J. Phys. Chem. A **107**, 10497 (2003).
[52] P. L. Pohjonen and J. Koskikallio, Acta Chem. Scand., Ser. A **33**, 449 (1979).
[53] N. L. Arthur and T. N. Bell, Rev. Chem. Intermed. **2**, 37 (1978).
[54] W. H. Miller, N. C. Handy, and J. E. Adams, J. Chem. Phys. **72**, 99 (1980).
[55] K. Morokuma and S. Kato, in *Potential Energy Surfaces and Dynamics Calculations*, edited by D. G. Truhlar (Plenum, New York, 1981).
[56] E. Kraka and T. H. Dunning, *Advances in Molecular Electronic Structure Theory* (JAI, New York, 1990), Vol. I, p. 129.
[57] S. C. Tyler, H. O. Ajie, A. L. Rice, R. J. Cicerone, and E. C. Tuazon, Geophys. Res. Lett. **27**, 1715 (2000).
[58] O. Roberto-Neto, E. L. Coitiño, and D. G. Truhlar, J. Phys. Chem. A **102**, 4568 (1998).
[59] H. A. Michelsen, J. Geophys. Res. **106**, 12267 (2001).
[60] T. J. Wallington and M. D. Hurley, Chem. Phys. Lett. **189**, 437 (1992).
[61] G. D. Boone, F. Agyin, F. M. Tao, and S. A. Hewitt, Book of Abstracts, Proceedings of the 217th ACS National Meeting, Anahein CA, 1999 (unpublished) Abstract PHYS-299.
[62] Y. Matsumi, K. Izumi, V. Skorokhodov, M. Kawasaki, and N. Tanaka, J. Phys. Chem. **101**, 1216 (1997).
[63] G. Chiltz, R. Eckling, P. Goldfinger, G. Huybrechts, H. S. Johnston, L. Meyers, and G. Verbeke, J. Chem. Phys. **38**, 1053 (1963).
[64] G. Saueressig, P. Bergamaschi, J. N. Crowley, H. Fisher, and G. W. Harris, Geophys. Res. Lett. **23**, 3619 (1996).
[65] R. N. Porter and L. M. Raff, in *Dynamics of Molecular Collisions*, edited by W. H. Miller (Plenum, New York, 1976), Pt. B.
[66] D. G. Truhlar and J. T. Muckerman, in *Atom-Molecules Collision Theory*, edited by R. B. Bernstein (Plenum, New York, 1979).
[67] L. M. Raff and D. L. Thompson, in *Theory of Chemical Reaction Dynamics*, edited by M. Baer (CRC, Boca Raton, 1985), Vol. 3.
[68] W. L. Hase, R. J. Duchovic, X. Hu *et al.*, VENUS 96, a general chemical dynamics computer program; QCPE Bull. **16**, 43 (1996).
[69] S. F. Wu and R. A. Marcus, J. Phys. Chem. **53**, 4026 (1970).
[70] J. M. Bowman and A. Kuppermann, J. Chem. Phys. **59**, 6524 (1973).
[71] D. G. Truhlar, J. Phys. Chem. **83**, 18 (1979).
[72] G. C. Schatz, J. Chem. Phys. **79**, 5386 (1983).

[73] D.-H. Lu and W. L. Hase, J. Chem. Phys. **89**, 6723 (1988).
[74] A. J. C. Varandas, J. Brandao, and M. R. Pastrana, J. Chem. Phys. **96**, 5137 (1992).
[75] A. J. C. Varandas and J. M. C. Marques, J. Chem. Phys. **100**, 1908 (1994).
[76] A. J. C. Varandas, Chem. Phys. Lett. **225**, 18 (1994).
[77] M. Ben-Nun and R. D. Levine, J. Chem. Phys. **101**, 8768 (1994).
[78] X. Wang, M. Ben-Nun, and R. D. Levine, Chem. Phys. **197**, 1 (1995).
[79] M. Ben-Nun and R. D. Levine, J. Chem. Phys. **105**, 8136 (1996).
[80] D. A. McCormack and K. F. Lim, Phys. Chem. Chem. Phys. **1**, 1 (1999).
[81] G. Stock and U. Müller, J. Chem. Phys. **111**, 65 (1999).
[82] U. Müller and G. Stock, J. Chem. Phys. **111**, 77 (1999).
[83] J. M. C. Marques, E. Martinez-Nuñez, A. Fernandez-Ramos, and S. Vazquez, J. Phys. Chem. **109**, 5415 (2005).
[84] R. J. Duchovic and M. A. Parker, J. Phys. Chem. **109**, 5883 (2005).
[85] J. C. Gray, D. G. Truhlar, L. Clemens, J. W. Duff, F. M. Chapman, G. O. Morrell, and E. F. Hayes, J. Chem. Phys. **69**, 240 (1978).
[86] R. D. Levine and R. B. Bernstein, *Molecular Reaction Dynamics and Chemical Reactivity* (Oxford University Press, New York, 1987).
[87] M. Ben-Nun, M. Brouard, J. P. Simons, and R. D. Levine, Chem. Phys. Lett. **210**, 423 (1993).
[88] G. C. Schatz and J. Ross, J. Chem. Phys. **66**, 1037 (1977).
[89] M. J. Bass, M. Brouard, C. Vallance, T. N. Kitsopoulos, P. C. Samartzis, and R. L. Toomes, J. Chem. Phys. **119**, 7168 (2003).
[90] S. Rudic, C. Murray, J. N. Harvey, and A. J. Orr-Ewing, J. Chem. Phys. **120**, 186 (2004).
[91] G. Nyman, H.-G. Yu, and R. B. Walken, J. Chem. Phys. **109**, 5896 (1998).
[92] H.-G. Yu and G. Nyman, J. Chem. Phys. **110**, 7233 (1999).
[93] H.-G. Yu and G. Nyman, Phys. Chem. Chem. Phys. **1**, 1181 (1999).
[94] H.-G. Yu and G. Nyman, J. Chem. Phys. **111**, 6693 (1999).
[95] S. Skokov and J. M. Bowman, J. Chem. Phys. **113**, 4495 (2000).
[96] D. Troya, J. Millan, I. Baños, and M. Gonzalez, J. Chem. Phys. **117**, 5730 (2002).
[97] J. Zhou, B. Zhang, J. J. Lin, and K. Liu, Mol. Phys. **103**, 1757 (2005).
[98] L. Bonnet and J. C. Rayez, Chem. Phys. Lett. **277**, 183 (1997).
[99] L. Bañares, F. J. Aoiz, P. Honvault, B. Bussery-Honvault, and J.-M. Launay, J. Chem. Phys. **118**, 565 (2003).
[100] A. E. Pomerantz, F. Ausfelder, R. N. Zare, S. C. Althorpe, F. J. Aoiz, L. Bañares, and J. F. Castillo, J. Chem. Phys. **120**, 3244 (2004); T. Xiao, J. Bowman, J. W. Duff, M. Braunstein, and B. Ramachandran, *ibid.* **122**, 014301 (2005).
[101] B. D. Dean, J. D. Ayers, F. Fernandez-Alonso, and R. N. Zare, J. Chem. Phys. **116**, 6634 (2002).
[102] B. D. Dean, F. Fernández-Alonso, and R. N. Zare, J. Phys. Chem. A **105**, 2228 (2001).
[103] D. A. V. Kliner, K.-D. Rinnen, and R. N. Zare, Chem. Phys. Lett. **166**, 107 (1990).
[104] D. P. Gerrity and J. J. Valentini, J. Chem. Phys. **81**, 1298 (1984).
[105] D. G. Truhlar and N. C. Blais, J. Chem. Phys. **67**, 1532 (1977).
[106] S. Yoon, S. Henton, A. N. Zirkovic, and F. F. Crim, J. Chem. Phys. **116**, 10744 (2002). The value 10±5 is derived in the present work from the results in this reference for the symmetric and asymmetric stretching results.
[107] J. C. Polanyi, Acc. Chem. Res. **5**, 161 (1972).
[108] J. Sansón, J. C. Corchado, C. Rangel, and J. Espinosa-García, J. Chem. Phys. **124**, 074312 (2006).
[109] H. A. Bechtel, J. P. Camden, D. J. A. Brown, and R. N. Zare, J. Chem. Phys. **120**, 5096 (2004).
[110] See EPAPS Document No. E-JCPSA6-124-001611 for the optimized geometries and energies of all stationary points using the PES-2005 surface. This document can be reached via a direct link in the online article's HTML reference section or via the EPAPS homepage (http://www.aip.org/pubservs/epaps.html).